Analysis & Improvement of railway crossing

Using explicit Finite Element simulations

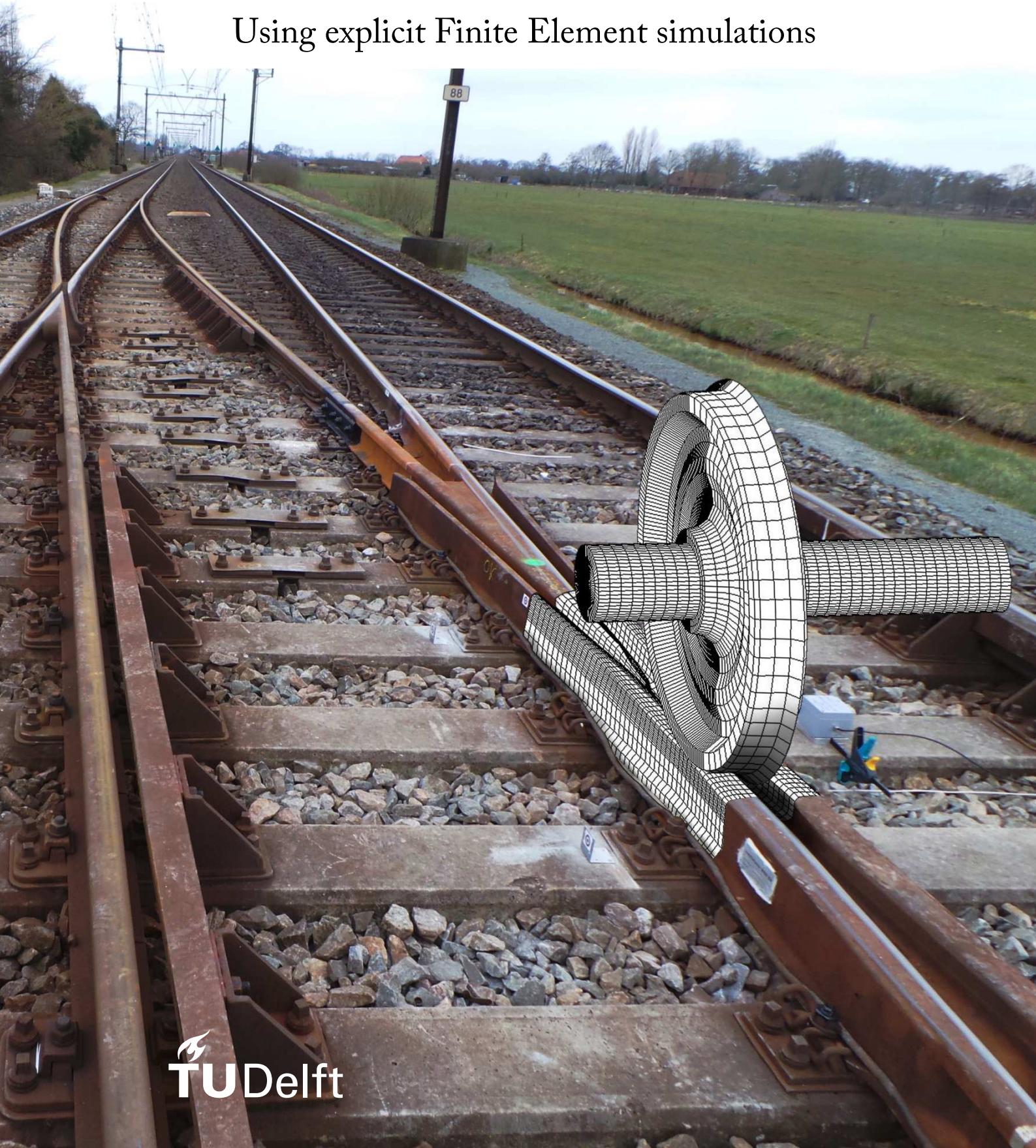

TU Delft

Analysis and improvement of railway crossing
Using explicit Finite Element simulations

By

A.A. Mashal

In partial fulfilment of the requirements for the degree of

Master of Science
in Structural Engineering

at the Delft University of Technology,
to be defended publicly on Tuesday July 13, 2016 at 15:45.

Promoter:	Prof. dr. ir. R.P.B.J. Dollevoet,	TU Delft
Thesis committee:	Dr.ir. V.L. Markine,	TU Delft
	Dr. ir. P.C.J. Hoogenboom,	TU Delft
	MSc. Y. Ma,	TU Delft
	Ing. S. Bömers,	Strukton B.V.

Preface

بِسْمِ ٱللَّهِ ٱلرَّحْمَٰنِ ٱلرَّحِيمِ

In the name of Allaah, the Most Gracious, the Most Merciful

All the praises and thanks be to Allaah, the Most High, Who guided me and made it easy upon me to complete this MSc project, through which I gained many benefits and pleasant memories.

Besides, I am grateful to Professor Rolf Dollevoet for his stimulation and support and providing me the chance to attend the Railway Conference 2016, where I had the opportunity to present some of my results which are also described in this report.

I would like to thank Valéri Markine for introducing me to the field of Railway Engineering, supervising my work and providing me with equipment and facilities with which I could complete this work.

Special thanks to my colleague and advisor, Yuewei Ma, for sharing his knowledge with me and for the many interesting discussions that we had about research and other than that. We were indeed a good team, it is a pity that our ways will split from here on.

Also, my thanks go to my other committee members, Pierre Hoogenboom and Stefan Bömers, for their encouragement and helpful comments on the drafts of my thesis.

Last but not the least, I would like to express my sincere gratitude to my family and especially my mother for her continuing support and encouragement, whose love and care have been a constant source of motivation for me.

The research described in this thesis was carried out at the Faculty of Civil Engineering, Department of Structural Engineering at the Section of Railway Engineering during the period November 2015 to July 2016.

Abdul Ahad Mashal
Delft, July 2016

Contents

Abstract

Railway crossings are one of the most important and vulnerable components in railway network. Nowadays, due to intensive use of the track together with higher train speeds and heavier axle loads, more and more problems associated with crossings are reported and it is continuing to be an important factor limiting its service life.

In this MSc thesis, a realistic 3D finite element (FE) model of the crossing panel is developed to analyse the stress state arising from the impact event and, providing recommendations on how to effectively mitigate the impact loads. The scenario which is simulated and studied in this report is that of a train wheel passing a railway crossing in the facing as well as in the trailing direction. Prior to the FE modelling, first, 2D-geometric contact analysis is performed calculating all the contact properties at the wheel-rail interface. The obtained contact properties are then used as guidance during the FE modelling to implement adaptive mesh refinement at the running band of the wheel in order to get accurate solution of the rolling contact stresses.
From the FE simulation results, high impact forces can be observed in the transition zone of the crossing. The detailed surface and subsurface stress analysis reveals that these forces generate high contact stresses subsequently causing yielding of the materials and intense plastic strain accumulation.

Verifications and validations are carried out to examine whether the results from the FE model are correlating with the reality. From them, attention has been paid to minimize undesirable effects of the boundaries and to verify the convergence of the solution. Besides, the response of the FE model is validated against the field experiment of the axle box and the crossing nose accelerations.

Thereafter, a parametric study is performed to investigate the influence of some interesting case studies on the magnitude of the impact loads. In this regard, a comparison of the contact properties utilizing elastic and plastic material models showed conformities as well as discrepancies in the stress state for these two material models. Besides, several cases studies have been carried out on the vertical substructure stiffness variation and geometric design modification of the crossing panel. From this it can be concluded that the investigated case studies provide interesting opportunities to reduce effectively the impact forces on the crossing. Moreover, a comparison between facing and trailing direction has managed to identify the impact force behaviour for these two different operational conditions.

So in short, the FE model is thus capable to solve the wheel-crossing contact stress problem at the crossing and it is flexible enough to examine the influence of design modifications on the impact force and its resulting stress state under different operational conditions.

Keywords: wheel-rail interface interaction, 2D geometric analysis, 3D explicit FEM, railway crossing, transition.

1. Introduction

1.1. General

A railway turnout is built to control the traffic flow on the railway network. It enables the train to switch between two intersected tracks, see Figure 1a. Railway turnouts, especially the crossings are some of the most essential and maintenance demanding components of railway infrastructure. The complex rail geometry and the track discontinuity results in the amplification of wheel loads at the crossing nose. Repeated high impact loads from passing trains leads to excessive wear, severe plastic deformation and cracks which will further exacerbate the spalling damage or even to sudden fracture of the crossing nose. Nowadays, the Dutch railway network suffers from these problems to such a high degree that it has been reported that the particular crossing shown in Figure 1b-d needs to be urgently repaired every half year.

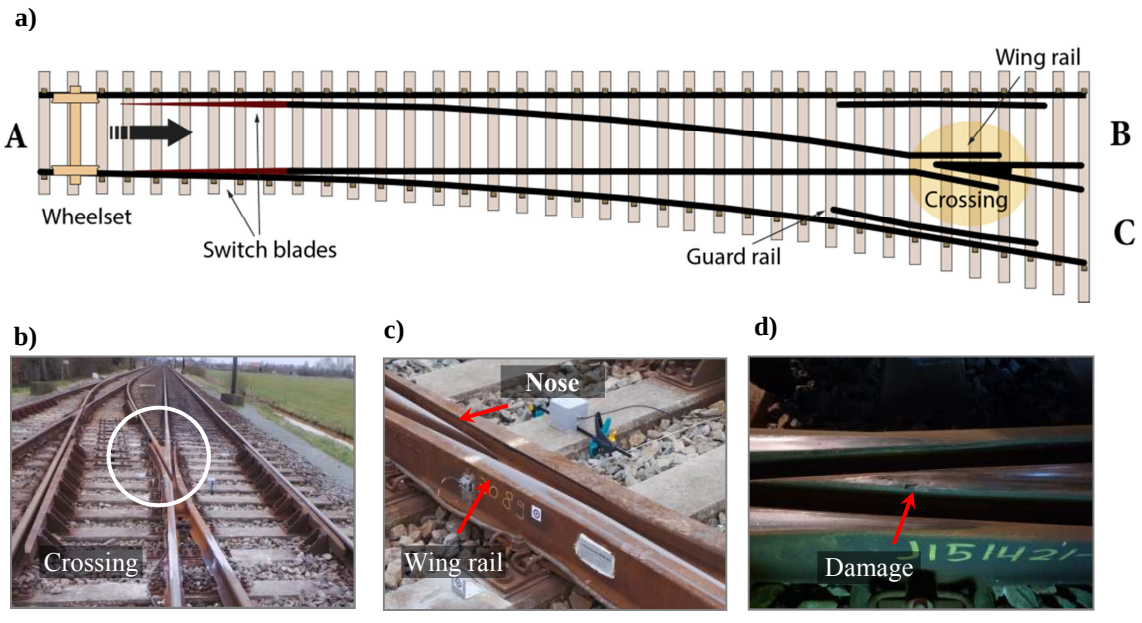

Figure 1. a) Railway turnout overview and description of the track components.
b) A typical turnout in the Dutch railway network. c) Crossing panel, d) Damage at the crossing nose

1.2. State of art

In order to prevent the catastrophic consequences of sudden failure and to manage an appropriate maintenance operation of the turnout components, detailed knowledge of the wheel-crossing interaction appears to be of critical importance both in academic research and for engineering applications. In this regard, numerical simulations are an insightful tool for analysing complicated dynamic problems. Over the past decades, significant progress has been made in accelerating the numerical simulations for wheel-crossing interaction. However, there are only a limited number of geometric contact models [1,18] which are able to assess wheel and turnout contact interaction. Besides, only few of the developed numerical models [2-5] actually take into account the realistic wheel and turnout contact geometries together with nonlinear material properties.

1.3. Objective of this research

The goal of this MSc project is to develop numerical models for simulating the dynamic impact between a wheel and a crossing panel in order to analyse its resulting stress state, and to provide some measures which can mitigate the high impact loads. In this thesis the following research questions are answered:

- What is the contact force and stress distribution at the crossing nose resulting from an impact event?
- What are the influences of the vertical track stiffness and crossing shape modification on the contact forces and its resulting stress state?
- What is the difference of the contact force distribution between facing and trailing operations?

1.4. Scope of this research

The main focus of this report will be laid on wheel-rail interaction at a railway crossing. Figure 1a illustrates the layout of the turnout including the crossing which is studied in this work. Basically, there are two main directions in which the trains can travel, namely in the through and the divergent path. An example of the through direction is the traveling route from A to B which is called the facing direction. Traveling in the opposite directions (from B to A) is called trailing direction. This distinction is important because the wheel-rail interaction for these two directions is different. In practice it has been observed that the traffic flow in the facing direction usually results in severe damage on the crossing nose. In order to analyse and improve wheel-rail interaction at the crossing, numerical simulations are performed later in this work for both facing direction and trailing direction.
In reality, the train can also travel from A to C which is on a divergent path. Although the developed models are capable to simulate this case as well, due to the time frame of this MSc project the divergent direction is not considered here.

1.5. Structure of this thesis

The (main) structure of this thesis is as follows: Sections 2, provides a literature overview of the existing numerical contact models to investigate the wheel-rail interaction. The discussion in this section will serve as theoretical framework for the following parts where the wheel-rail contact analyses is considered.

Following that, Section 3 presents, the computational strategy, which combines a 2D (static) geometric contact model, and a 3D (dynamic) finite element contact model, incorporating realistic material properties as well as real wheel and crossing profiles to accurately simulate the impact in the transition zone.

After the verification and validation of the developed models with the field measurements in Section 4, a parametric study is carried out in Section 5 in which comparison of the contact stresses between elastic vs plastic material properties are presented. Besides, the influences of superstructure stiffness, geometric crossing shape modification and facing-trailing directions on the impact event are discussed as well. Finally, the conclusions and suggestions are presented in Section 6.

2. Theoretical background

2.1. Wheel-rail interaction

One of the most important and complicated aspects of railway engineering is wheel-rail interaction, especially at a railway crossing. Vehicle kinematics at such crossing results in an impact event generating high contact forces which is highly complex and nonlinear phenomenon. Prior to discuss how this problem is tackled, first, some basic principles of rolling contact mechanics will be introduced which will serve as a theoretical framework for the following sections. This section begins with basic consideration of contact forces arising at the wheel-rail interface due to the frictional rolling contact. In the succeeding discussions, some of the available tools to assess these contact forces and their resulting stress state are described. Finally, this section ends with a literature review on computational strategies on how to implement efficiently different numerical tools to assess wheel-rail contact problem.

2.1.1. Frictional rolling contact mechanics

When a vehicle is running along the track, contact forces arise at the point of contact with the rails. The main challenge is to solve accurately these contact forces at wheel-rail interface. These contact forces can be divided into normal and tangential components. The normal force represents the vertical force while the tangential force contains the lateral as well as the longitudinal force. In order to discuss this in more detail, a classical example is considered in which the wheel is rolling on a smooth rail surface as illustrated in Figure 2. The wheel is rolling with a radius ***R***, forward velocity ***V*** and angular velocity ***ω***. Consequently, the angular velocity will generate circumferential velocity **ωR**.

Under stationary conditions, normal contact force $\boldsymbol{F_v}$ is the product of gravity acceleration and the car body mass. For simplicity the lateral force is neglected here since the problem is discussed in a 2D plane. In order to maintain the wheel traveling speed a tractive effort (torque ***M***) is required. The application of traction on the wheel will introduce a reactive longitudinal tangential force $\boldsymbol{F_t}$ at the point of the wheel-rail contact.

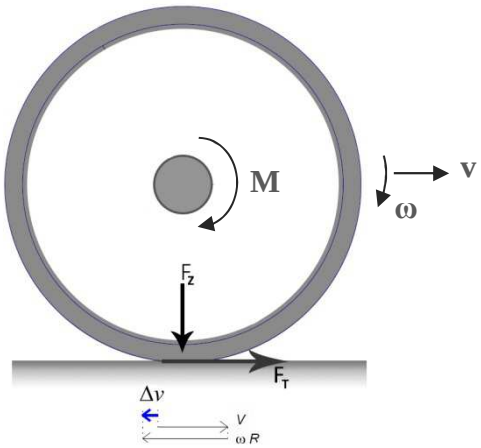

Figure 2: free body diagram of a rolling wheel with relative motion at the contact surface

Due to the deformation of the contacting bodies at the point of contact, a contact patch develops which will result in the formation contact stresses. The size and shape of the contact patch depends on the normal force, the material properties as well as the geometry of the wheel and the rail in this region. Due the traction effort, the circumferential velocity **ωR** can be higher than the forward velocity ***V*** so that a small difference arises between the two velocities at the contact area. The relative difference in motion ***Δv*** is the so called ‘creepage’ indicating that at some places at the contact patch the two bodies are sliding relative to each other. This was first presented by Carter in 1926 [6] and is illustrated in Figure 3. It was shown that theoretically when creepage is zero no tangential force is transmitted and the whole contact area is in full sticking state. The maximum tangential force which can be transmitted is limited by Coulomb's friction law, which is equal to the product of the friction coefficient and the normal force. In this linear part of the curve the contact area can be divided into stick and slip regions. With increasing the tangential force through increase of traction effort, a slip region occurs at the rare of the contact

patch and spreads forward through the contact area decreasing the stick region, resulting in a rolling and sliding contact. When the tangential force reaches its saturation value, the stick region disappears, and the entire contact area is in a state of pure sliding. In practice, pure rolling is hardly to occur because of continuous need for braking and accelerating operations which means that wheel-rail interface is always in partial rolling and sliding conditions.

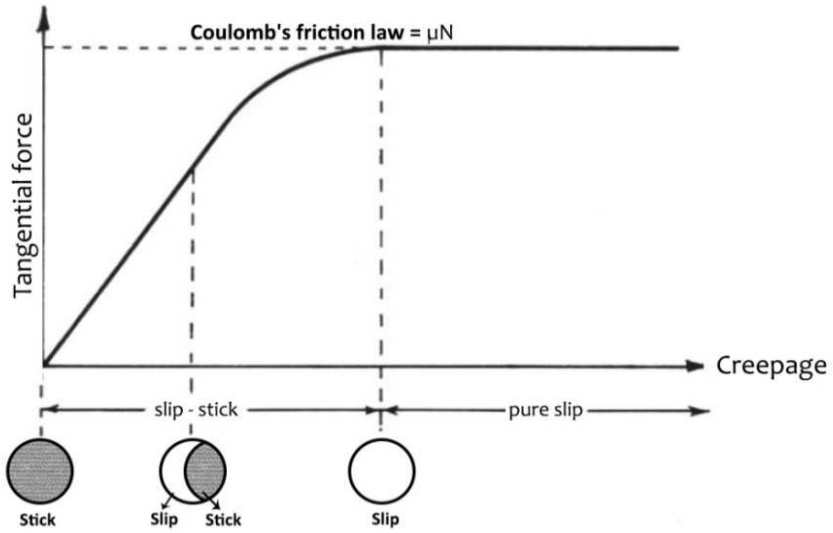

Figure 3: traction curve

Frictional rolling contact is very complicated because it involves nonlinear geometries and nonlinear material properties which make it impossible to solve the contact problem through analytical solutions. The next section describes some methods which are able to solve the wheel-rail contact problem through discretization of the contact patch and numerical calculations.

2.2. Numerical contact models

For the calculation of contact forces occurring at the wheel-rail interface, as discussed in the previous page, it is impossible to calculate it by hand. Fortunately, with the recent development of numerical simulation techniques and computer power it has become possible to tackle complicated wheel-rail interface problems. Nowadays, there is a large variety of algorithms [7-9] which can solve the normal and tangential contact force and provide detailed description of the contacting surfaces. This section presents a literature overview related to two often-used numerical tools for calculating wheel-rail contact conditions, namely the Multibody System (MBS) and the Finite Element Method (FEM). Historically due to limitations of the software tools, vehicle and track dynamics were investigated separately. MBS was developed to study the dynamic behaviour of vehicles while railway track models were usually based on FEM[10]. Both have their advantages and limitations and can provide an improved understanding of different aspects of the wheel and rail interaction.

2.2.1. Multibody System

In the MBS model, the whole train and the track are represented through a system of springs, masses and dashpots elements as shown in Figure 4. The track together with irregularities, curves, switches and crossings can be modelled for several kilometres. MBS can give the vehicle dynamic response like normal and tangential forces at each contact with the rails. Also the shape and size of the contact patch together with a detailed description of the contact pressure and traction can be provided.

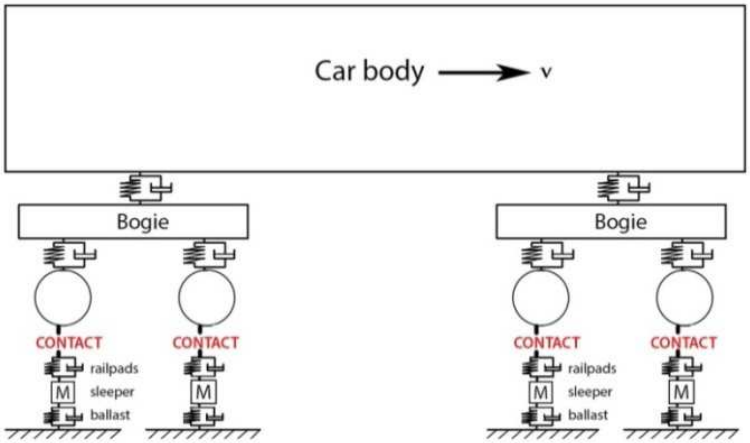

Figure 4: Multibody model. Taken from [10]

The dynamic behaviour of a multibody system is attained by solving equations of motion for the mass-spring system. There are a variety computation algorithms implemented in to the Multibody software to solve the contact problem between wheel and rail extremely fast. In this regards, some well-known theories are worth mentioning.

Hertz's Theory

In predicting the contact patch as well as the contact stresses, Heinrich Hertz was the first who published his work[11] in 1882 on the calculation of normal contact stresses. His contact model describes analytically what happens when two curved surfaces come in contact and deform slightly under the imposed loads. It gives the contact stress as a function of the normal contact force, the radii of curvature of both bodies and the modulus of elasticity and the Passion ratio of both bodies.
The following assumptions are made in determining the solutions of Hertz contact problem:

- The bodies are purely elastic (no plastic deformation)
- The surfaces are continuous and non-conforming.
- The bodies are in frictionless contact (perfectly smooth contact surface)
- Each body is considered to be half-space, (the area of contact is much smaller than the characteristic radius of the body)

Since Hertz's theory assumes that the bodies are perfectly smooth which indicates that there is no frictional contact, and thus it deals only with the normal stress. The contact patch is always an ellipse with parabolic stress distribution as shown in Figure 5.

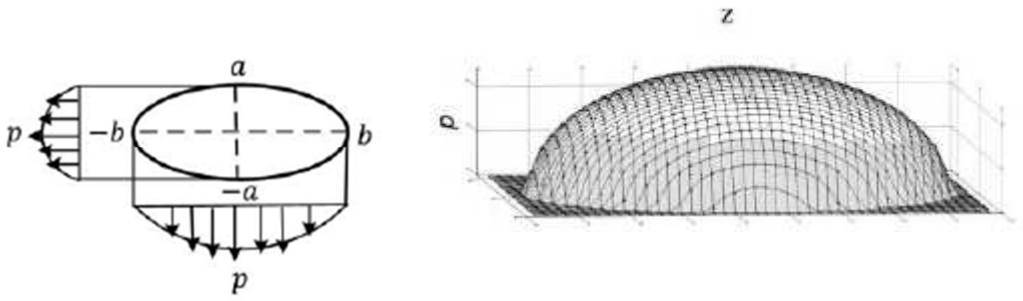

Figure 5: Hertz normal stress distribution. Taken from[12]

Kalker's Theory

Hertz theory is a good and relatively simple approach to calculate contact stresses, however in railway application the above mentioned assumptions are quite often violated which results in poor representation of the normal stresses. Especially, the assumption of constant curvature throughout the contact patch is not true for worn wheel and rail profiles. Besides, the half space assumption is questionably in case of wheel flange gauge contact because the contacting bodies may be of similar dimension to the contact area.

New models have been developed which some are modification of the Hertz's theory and others are based on different approach which are able to calculate contact stresses more accurately. In this regard, the most well-known and widely used is Kalker's theory of exact three-dimensional (3D) rolling contact[7]. Similar to Hertz's theory, Kalker assumes wheel and rail bodies as elastic half-spaces with pure elastic material properties. However, unlike Hertz's theory it is able to deal with non-elliptic and multi-contact patches cases very accurately [12], see also Figure 6. Moreover, it does not solve only the normal problem but it can also solve the tangential problem and give a description of the amount of creepage within the contact patch.

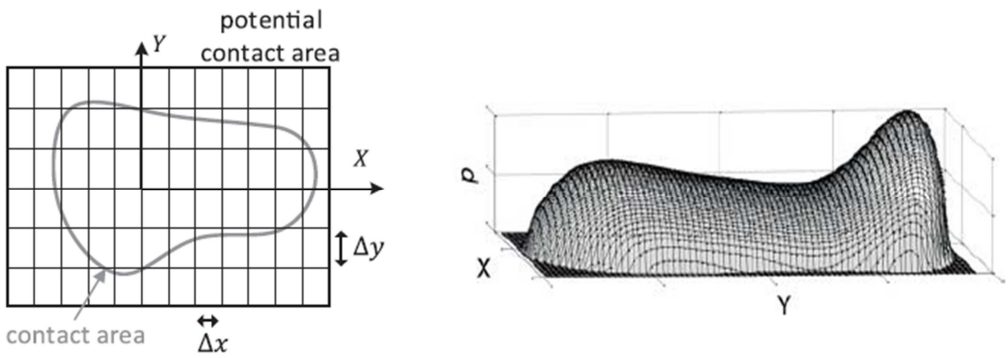

Figure 6: Kalker's theory Taken from[12]

Kalker's exact three-dimensional (3D) rolling contact theory has been implemented in software called CONTACT. The contact patch is discretized into small rectangular to evaluate the contact conditions and the contact stress for each strip finally ensuring a balance between the wheel load and the total normal force at the contact patch. However, due to this, CONTACT is so much computation expensive that it is not suitable to incorporate it into MBS software where fast calculation of the contact problem is required. Therefore, alternative algorithms have been introduced to solve faster the contact problem. Most notable in this regard is the simplified theory, the so called FASTSIM algorithm[13] . Nowadays, the algorithm has been implemented and widely used in MBS programs like SIMPACK[14]. Since the FASTSIM algorithm is an approximation of Kalker's exact theory it does contain certain errors. Kalker himself estimates the maximum error of 15% for some extreme cases[7].

In short, it can be concluded that although MBS is often used simulating wheel-rail response, it should be noted that the underlying theories which calculates the contact properties assumes rigid bodies or having linear elastic material properties. These assumptions can have an influence on the calculation results especially during the impact event. Therefore, the enhanced wheel-rail contact model to detect detailed contact properties at the impact moment should not be limited by these common simplifying assumptions for predicting material degradation. Especially in the transition region of the crossing where material plastification is likely to occur.

2.2.2. Finite Element Method

During recent years much attention has been paid to the improvement of the solution of the general wheel-rail contact problem. In this regard FEM has offered the possibility of detailed modelling which enables analysis of realistic 3D wheel-rail geometries, see for example Figure 7. It is also possible to use plastic material attributes to account for plastic deformation and to utilize more advanced frictional models than the Coulomb's friction law. Moreover it is not limited by linear theories like Hertz theory or half space assumptions which are present in most of the MBS calculations.

In FEM calculations a structure is divided into multiple elements (finite elements) connected at the 'nodes' which hold the elements together. In each element three sets of equations are formulated: the compatibility equations, which relate the strains to the displacements, the constitutive equations, which relate the stresses to the strains, and the equation of motion. Solving these set of equations, depending on the mesh size, generally results in a quite accurate description of stresses and strains of the modelled parts. However, FEM has also some disadvantages and limitations. Although a complete track system with the rails, the sleepers, the ballast and the subgrade can be modelled, only a very small part of the track can be analysed. Besides, because contact stresses are of high magnitude in a rather small area, the mesh size in the potential contact area should be small enough in order to achieve the required accuracy. This makes the analysis computationally

time consuming because for each element an additional set of equations needs to be solved. Also it has been shown that results of the FEM analysis are dependent on the mesh size [15], which means that the mesh size should be chosen carefully in order to get accurate results. For simulating impact events, these limitations demands intensive modelling effort, but when it is done wisely, it can provide more accurate solution of the contact stresses compared with the MBS. Therefore, also in this work, FEM is utilizing to analyse wheel-crossing interaction and to assess the rolling contact stresses. More information about the modelling and calculation process will be presented in Section 3.

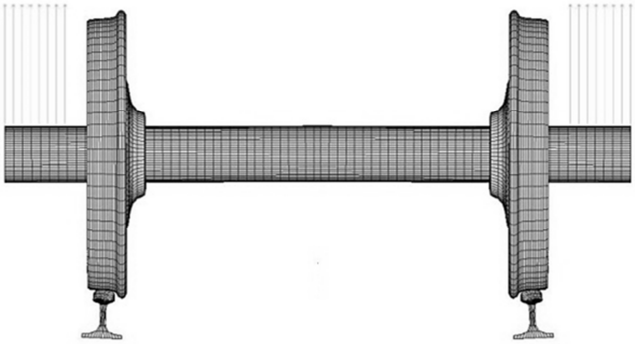

Figure 7: Wheel-rail FEM model [15]

2.3. Simulation methodologies

Compared with experimental studies, numerical simulations are cost effective and an insightful tool, which enables improvements to be made to design and materials. Due to this, numerical modelling has been of major focus of past and present researchers. For instance, Kassa et al. [16] addressed the dynamic interaction between train and railway turnout using two alternative numerical models. The first model is derived using a commercial MBS software GENSYS and the second model using the in-house software DIFF3D. The variation in rail profile is accounted for by sampling the cross-section of each rail at several positions along the turnout. Contact between the back of the wheel flange and the check rail, when the wheelset is steered through the crossing, is also considered. However, the crossing panel itself is simplified as a rigid structure.

Another approach was presented by Pletz et al.[17] where a finite element model for the simulating a wheel passing a crossing. The FE model consisting of one wheel, the wing rails and the crossing nose are used study the rolling/sliding behaviour between the wheel and crossing, impact loading, and equivalent plastic stress/strain at the different train speeds and in different passing directions.

Other researchers used a coupling strategy to combine the advantages of FEM and MBS. Jingmang et al. [18] used such an approach, where the effects of profile wear on the dynamic wheel–turnout interaction are studied using MBS and FEM software's. Both nominal and measured worn profiles are taken as inputs for the simulation. First, the geometric model is implemented to calculate the contact point distribution for certain longitudinal cross sections to analyse the effects of

profile wear. Then, a model of the vehicle and turnout are built in MBS software to simulate the dynamic response of the vehicle–turnout system. Finally, the finite element modelling of the wheelset on the switch, incorporated with plastic material model is implemented to assess contact forces and internal contact stresses. The lateral shifts of the wheelset and dynamic normal contact forces simulated in MBS are used as inputs parameters for FE model.

Predicting the damage of switches and crossing components was investigated by Johansson et al. [19], wherein the use of different numerical tools for the simulations including MBS and FEM has been made. For a given switch and crossing design with an initial set of rail profiles, MBS simulations have been performed to calculate wheel-rail contact forces, creepages and contact positions. Thereafter contact simulations with FEM were performed, taking into account the realistic material behaviour.

From the above literature review it can be concluded that a number of literature research have been produced in the past on the subject of simulation methodologies where in some cases different numerical methods are combined to achieve more complete models. Further on in this work, likewise, a coupling strategy for simulating wheel-turnout interaction is presented using 2D static geometric model and 3D dynamic FE model to analyse contact force and stress distribution during impact event. More information about this model will be given in the next coming sections.

3.

Modelling and simulation of wheel-crossing interaction

This section demonstrates the practical performance of the theoretical knowledge discussed in the previous section. The wheel-rail frictional rolling contact stress problem is solved using Finite Element Method (FEM). First, the implemented computational strategy is explained followed by discussion on how wheel-crossing interaction is modelled, taking into account all the fundamental considerations of transient rolling/sliding contact conditions. Finally, the simulation results including contact forces, surface and subsurface stress distribution will be presented.

3.1. Computational strategy for this work

As mentioned earlier, FEM requires intensive modelling effort. In order to make the modelling effort efficient and robust, a coupling strategy is followed as illustrated in Figure 8. Basically, the computational strategy is an interconnection between three well-known programs namely; AutoCAD, MATLAB and ANSYS (LS-DYNA), bringing about a realistic and flexible model that is parametrised in all the three levels.

First and foremost, standard wheel and crossing cross sections are drawn and parameterized in software packed Auto-LISP. Following that, the cross sectional data is imported in MATLAB for 2D geometric contact analysis. The algorithm implemented is able to detect all the contact properties including; the initial contact point location, the normal clearance and the roll angle at variable locations along the crossing panel, and for different lateral shifts of the wheelset. These obtained contact information is used in building and meshing the 3D finite element (FE) model in ANSYS. Thereafter, using the FE model, the impact event of the wheel on the crossing nose is reproduced through explicit simulations. The obtained dynamic stress/strain responses on the surface and sub-surface are then analysed. Once the FE model is verified with the reality, a parametric study will be performed analysing the influence of the vertical track stiffness and the crossing nose shape on the impact forces.

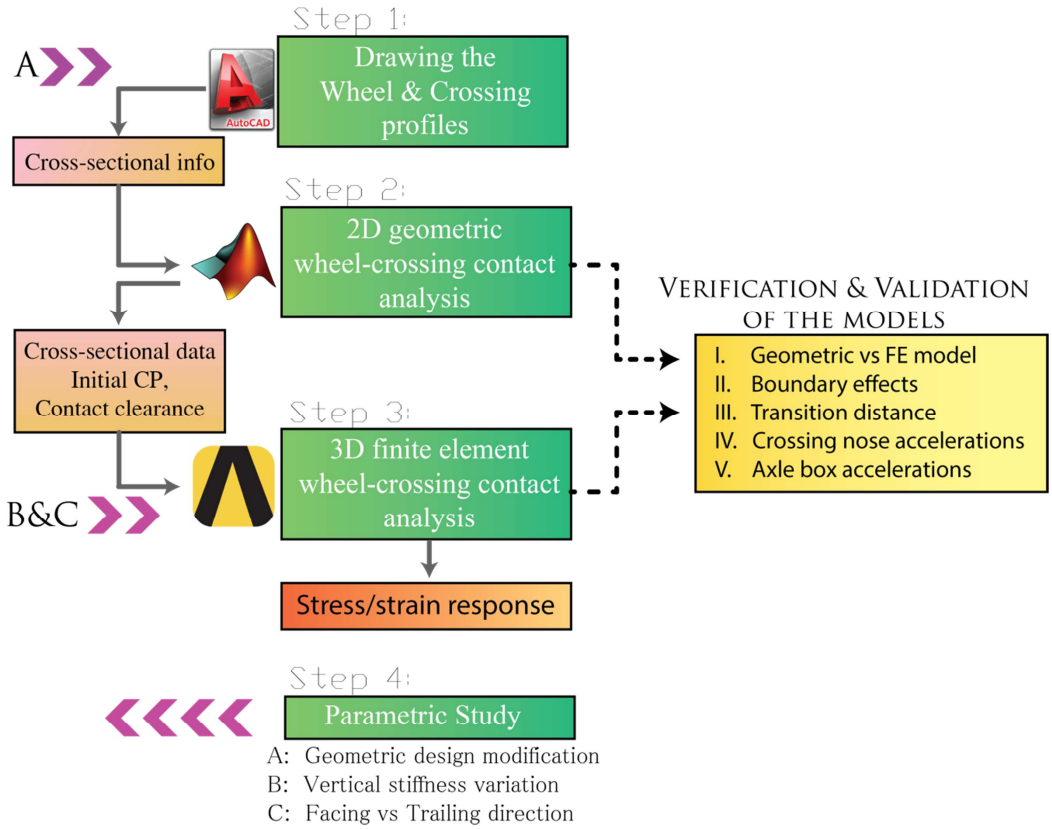

Figure 8: Flow chart of the computational strategy.

3.2. Wheel and crossing profiles used in simulations

As already mentioned, railway crossing is one of the most important component of the turnout. Such crossings, also known as the frogs, are specifically designed to ensure that the wheel is always supported by at least one rail so that the wheel can make a smooth transition from the wing rail to the nose rail. In order to prevent the wheel flange from striking the crossing nose, guard rails are installed to limit the lateral movement of the wheelset

Before discussing the details related to wheel-crossing modelling, first the wheel and crossing profiles are introduced from which the models are built. The crossing profile used in this work for numerical simulation is shown in Figure 9. It is a 1/9 crossing angle, which is the most used one in the Netherlands. It is prefabricated as a single unit and cast of manganese steel. According to the standard drawing as illustrated in Figure 9a-c, there are seven characteristic cross-sections, ranging from A to G, specifically used to describe the whole crossing geometry, see Appendix A for a complete overview of these cross sections.

At the two ends of the crossing panel, standard UIC54 normal rails (cross section AA) are integrated by stainless welds, see Figure 9a.

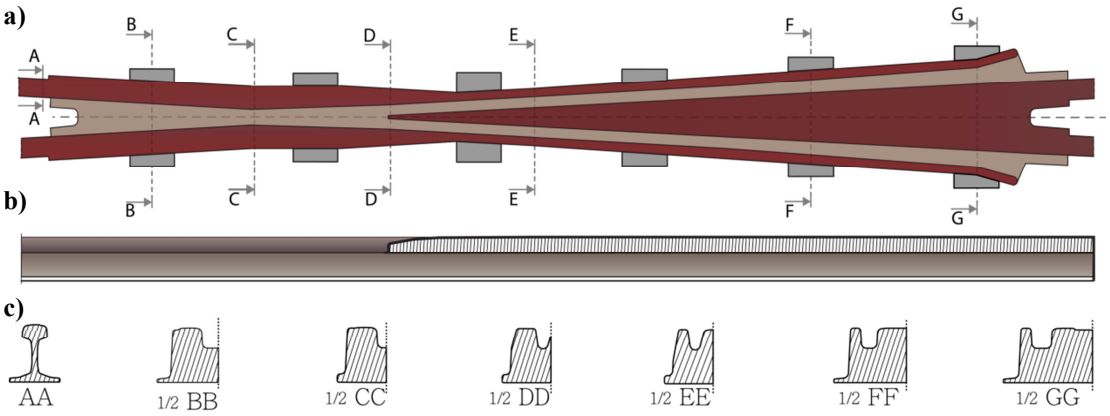

Figure 9: a) Crossing panel top view. b) Longitudinal cross section; c) Lateral cross-sections.

The vertical height of the crossing nose, as shown in Figure 9b, is designed to be gradually increased from DD to EE cross section. The overall length of the crossing is 2950 mm. It should be noted that, the wing rail profiles remain the same from BB until CC cross section, while it starts to shrink from CC to GG cross section. For the crossing nose, it expands both laterally and vertically along the path from DD to GG, and then split into two normal rails after GG.

The wheel model used in this work is a standard S1002 wheel profile [20] with a nominal rolling radius of 460mm. The inner gauge of the wheelset is 1360mm and the axle length is 2200mm. The wheel cross sectional drawing are shown in Figure 10 and are adopted from [21].

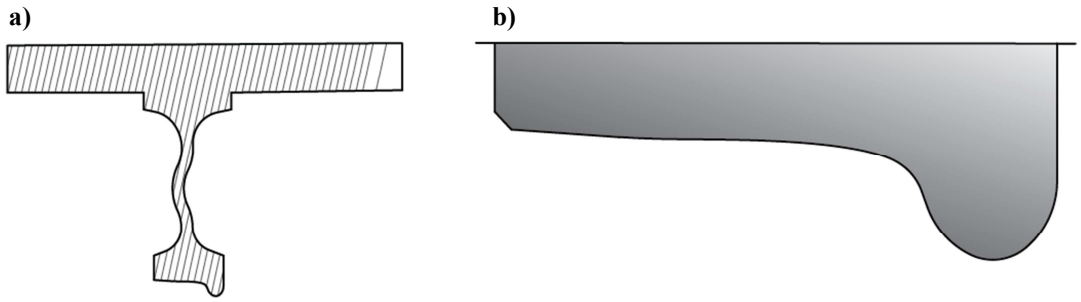

Figure 10: a) wheel cross section. b) Wheel tread zoom.

It can be observed from these standard wheel and rail profile drawings that the geometries are highly complex and nonlinear. The rapid cross sectional variations and discontinuities in the crossing geometry design, together with the conical shape of the wheel profile, constitute the roots of the problem thus resulting in an increased degradation of these components compared to regular tracks. A more in-depth discussion about the rolling contact between these geometries and the resulting contact stresses will be discussed in the coming subsections.

3.3. 2D-static geometric contact analysis

Analysing contact stress problems with finite element method (FEM) requires that the contact region at the wheel-rail interface is refined in order to capture the rolling contact stresses. However, in order to do that, the potential running band of the wheel should be known beforehand. Due to the complex crossing panel geometry it is not possible to estimate the possible contact region because the contact point location at the wheel-rail interface is changing continuously as the wheel is passing through the crossing. In order to investigate this contact locus variation, a detailed research on wheel and crossing geometries and their relative contact response is thus needed. In this current section, a 2D geometric contact model is developed to detect the potential contact point location at any position along the crossing panel which will be used as guidance during the FE modelling later on.

3.3.1. Computational process

As already mentioned, detecting potential contact point location is challenging for the nonlinear geometries but it is essential for simulation of wheel-crossing interaction. The algorithm implemented here to accomplish this challenge was initially developed by Ma [22] and it has been further extended in this work to be able to deal with complex geometries like the crossing.

In order to explain calculation process of the 2D geometric model, consider the 3D representation of a wheelset on a crossing panel as shown in Figure 11a. A global coordinate system O-XYZ is defined with its origin at the initial start of the crossing nose front. Besides, as second coordinate system at the centre of wheel axle O^w-$X^wY^wZ^w$, is defined which is movable along the crossing panel.

The characteristic cross sections of the crossing panel and the wheel are loaded in MATLAB and placed at their proper location according to the defined coordinate system. Additional cross sectional profiles, at the intermediate locations between the characteristic profiles are generated by longitudinal interpolation, see Figure 9b.

For any cross section at distance ***d*** from the location of the wheelset to the origin of the global coordinate system, contact simulation can be performed to achieve contact properties. Once the wheelset is placed at the desired position, the wheelset is shifted lateral with a prescribed lateral displacement ***dx***. Then the wheelset is rotated with multiple rotation angles. For each combination of a prescribed lateral displacement and a prescribed rotation angle, if both wheels stay in contact with the rail then that position is counted as a potential contact location. This process is repeated for the lateral shifts of 10 mm to the left and 10 mm to the right of the centreline with an increment of 1 mm.

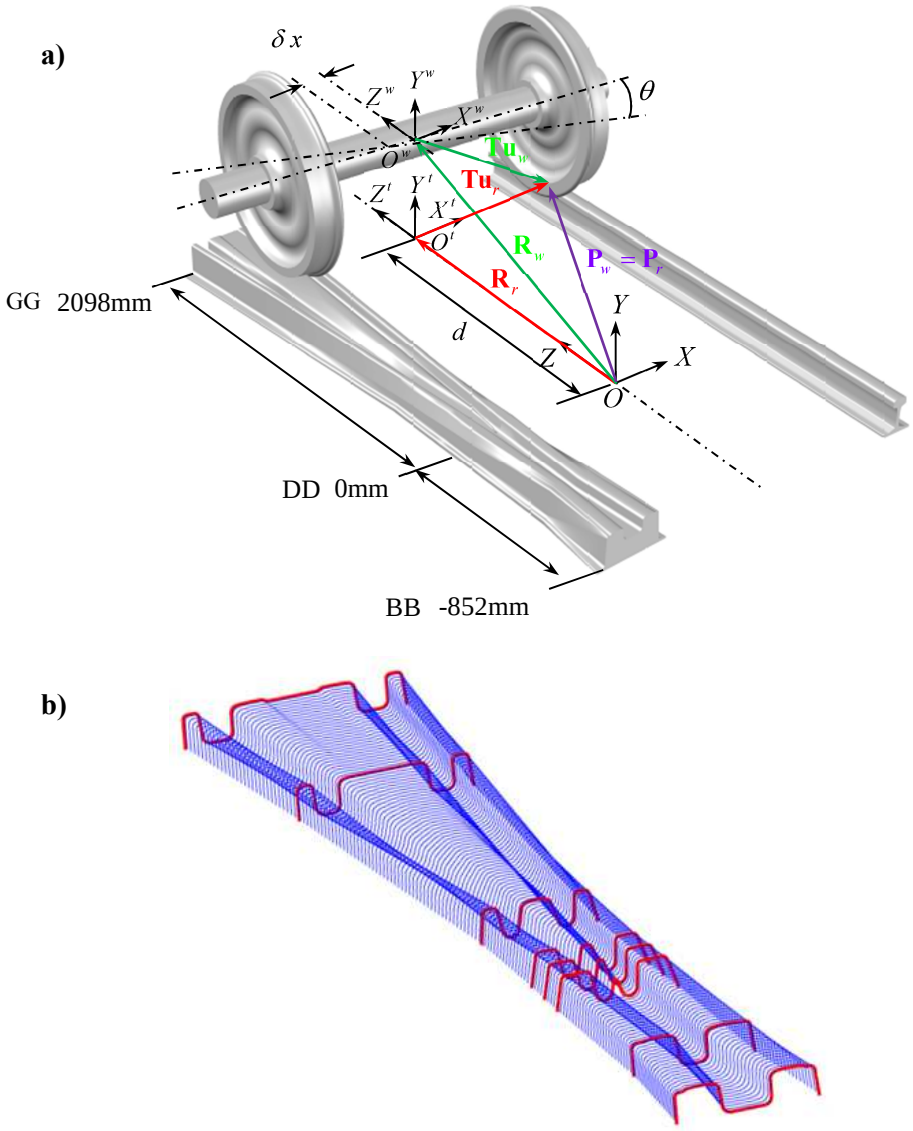

Figure 11: a) Wheel and crossing coordinate systems. b) Interpolated crossing cross section profiles between BB and GG cross sections

3.3.2. Contact simulation results

The geometric contact simulation procedure as described in the previous section is solved for all the characteristic cross sections and some additional interpolated cross sections. Depending on the amount of cross section for which contact simulation is performed, the obtained results including contact point location, normal contact clearance as well as the relative positions between wheel and rail are calculated within several seconds. Some of these results are presented in this subsection and some parts will be discussed in connection with the FE model in Section 3.4.

Single wheel-turnout cross section

The (main) feature of the geometric model is demonstrated by analysing a random cross section along the crossing panel as shown in Figure 12. Here, the wheelset is positioned at a distance of 180mm from the start of the crossing nose. It can be seen that only the bottom part of the wheelset is considered, with the crossing profile supporting the left wheel while the stock rail supporting the right wheel.

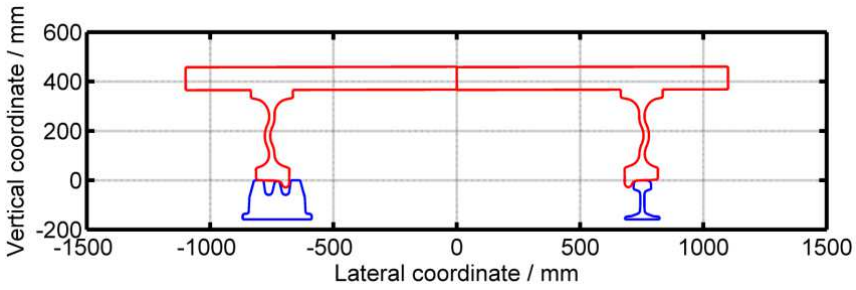

Figure 12: Wheel set located at interpolated cross section.

The figure above shows the situation for zero lateral shift of the wheelset in which the centreline of the wheelset is aligned with the centreline of the track. The lateral movement of the wheelset causes the contact point to change as it is shown in Figure 13a-b. From this figure it can be observed that for several possible lateral shifts of the wheelset the contact point on the wing rail is located at the same location. However because of the conical shape of the wheel, the contact point on the wheel profile is changing for the same lateral shifts. Besides, because of the conformal shape of the wheel with the crossing nose, it is clear that the contact point distribution is more uniform as compared with the wing rail.

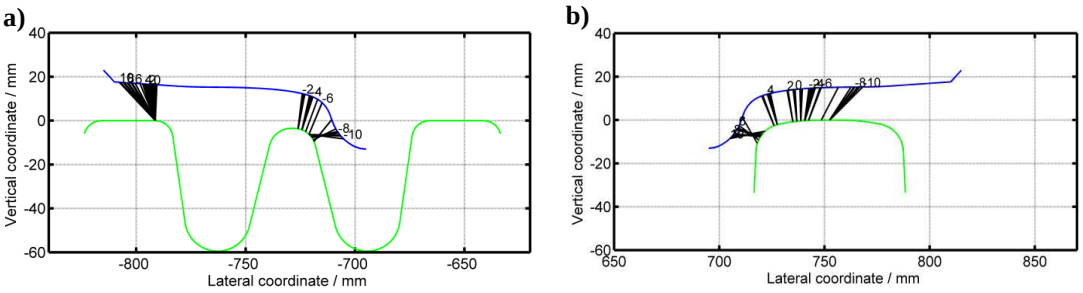

Figure 13: Contact point distribution under different lateral displacement. a).Left wheel-crossing interaction. b) Right wheel-stock rail interaction.

Different contact regimes

As the wheel is passing over a crossing, three different contact regimes are common to occur namely, I) single point contact on the wing rail, II) double point contact on both wing and crossing nose l, III) single point contact on the crossing nose, see also Figure 14. Contact regime II is the most important and critical part of the crossing panel because of the high impact loads which are generated due to transition process. An accurate description of the boundaries and the contact point location at these contact regimes are thus important for the refinement of the FE model. Figure 14b shows the contact regimes borders calculated with the geometric model. From this figure it is obvious to see that the contact regime II occurs at very short distance compared with the other two contact regimes.

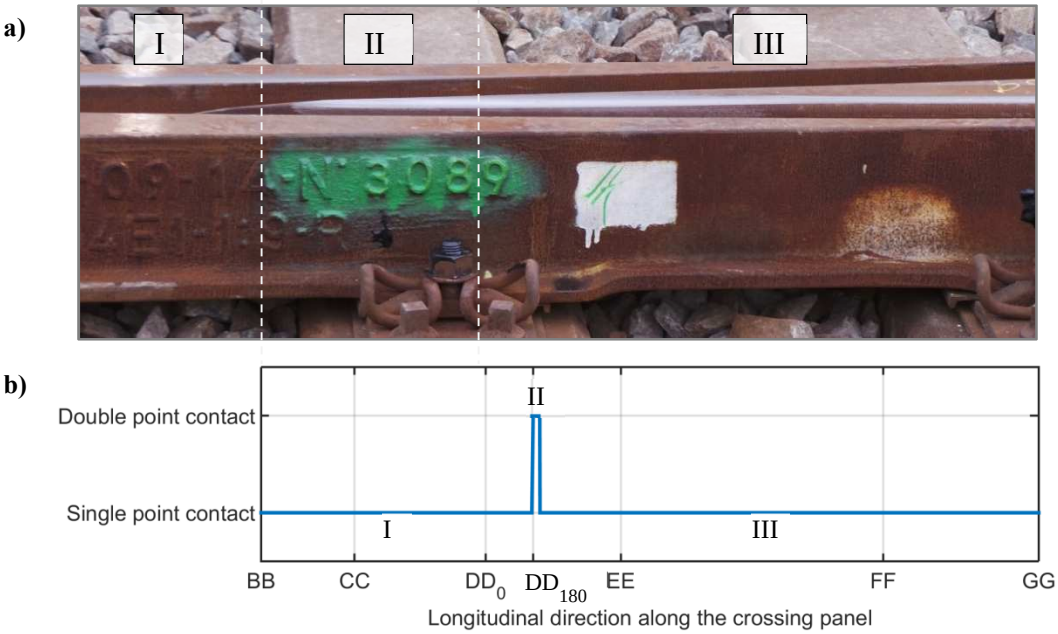

Figure 14: a) Different contact regimes; b) Calculated contact regimes for the crossing panel.

The boundaries of the different contact regimes are detected by calculating the normal contact clearance distribution between the wheel and the rail. Contact clearance is the normal distance between two points located at the contact surface between wheel and rail as illustrated in Figure 15a. For the three cross sections, DD_0, DD_180 and EE, the relative wheel-rail position as well as the contact clearances are shown in Figure 15. From Figure 15b-c it is clear that cross section DD_0 belongs to contact regime I because the contact clearance for the left wing rail is zero indicating that the wheel and the rail must be at contact this place. Moreover, for the same figure, the contact clearance at the crossing nose is larger than zero indicating thus the absence of contact at this location. From Figure 15d-e, it can be observed that the cross section DD_180 befits contact regime II due to the simultaneous double point contact at the wing rail and the crossing nose. After the double contact regime, again single point contact prevails at the crossing nose. This can be confirmed with Figure 15f-g, where the contact clearance for cross section EE is zero only at the crossing nose.

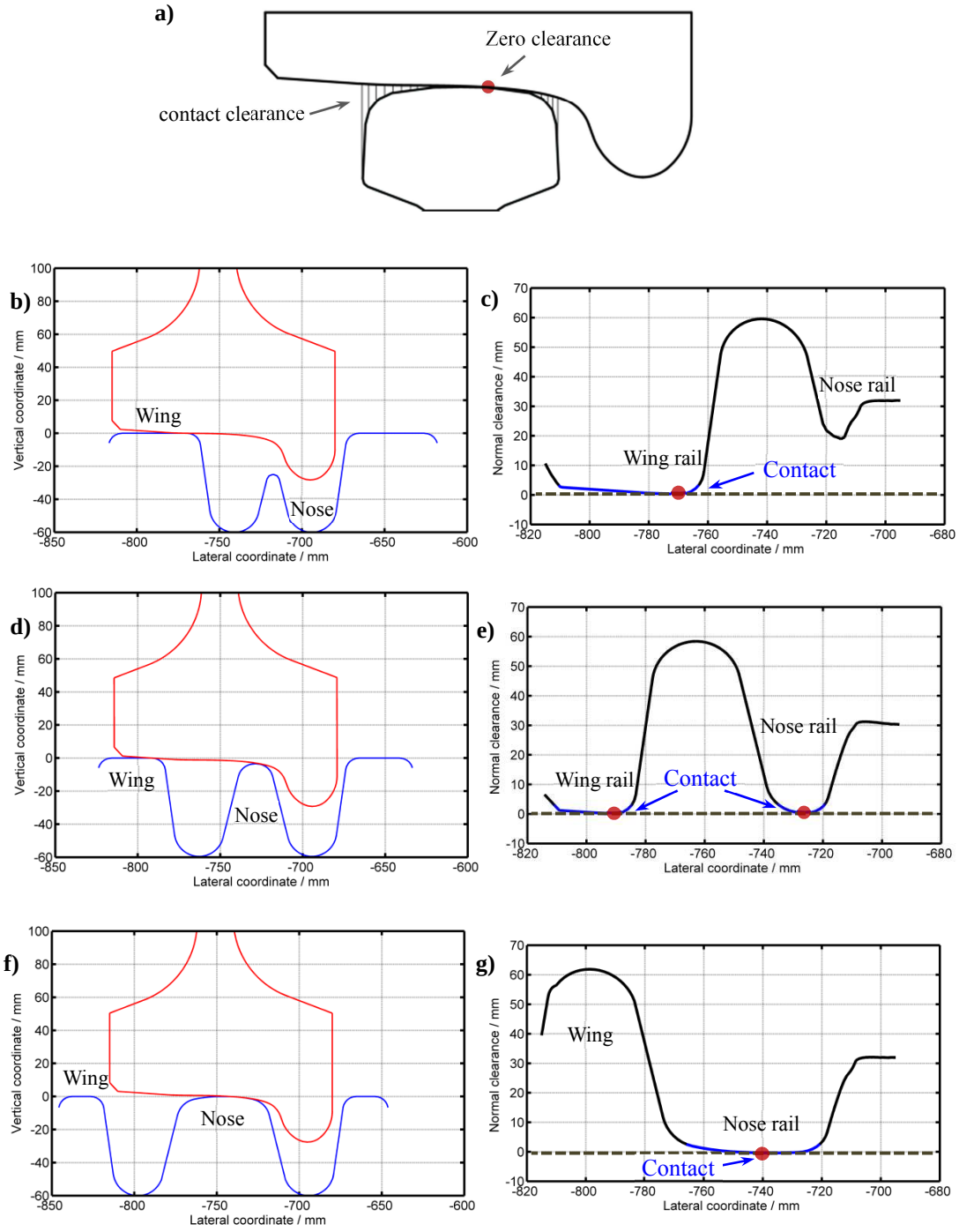

Figure 15: a) Definition of the normal contact clearance; b) Relative position of the wheel w.r.t. cross section ***DD_0***. c) Contact gap between the wheel and cross section ***DD_0***. d) Relative position of the wheel w.r.t. cross section ***DD_180***. e) Contact gap between the wheel and cross section ***DD_180***. f) Relative position of the wheel w.r.t. cross section ***EE***. g) Contact gap between the wheel and cross section ***EE***.

Vertical wheel trajectory along the crossing panel

From Figure 15, it was observed that the contact location at the wheel-rail interface is continuously changing when the wheel passes the crossing panel. Taking the wheel axle as a reference point, it is shown in Figure 16 that the wheel moves also in the vertical direction. Such oscillations can result in impact forces to occur on the crossing surface due to the vibration of the wheelset. From Figure 16 it can be seen that the maximum vertical displacement of the wheel (1.634mm) occurs at cross section ***DD_180*** which is 180 mm from the front of the crossing nose. This is consistent with Figure 15g where it can be seen that this particular cross section marks the initial stage of the transition zone.

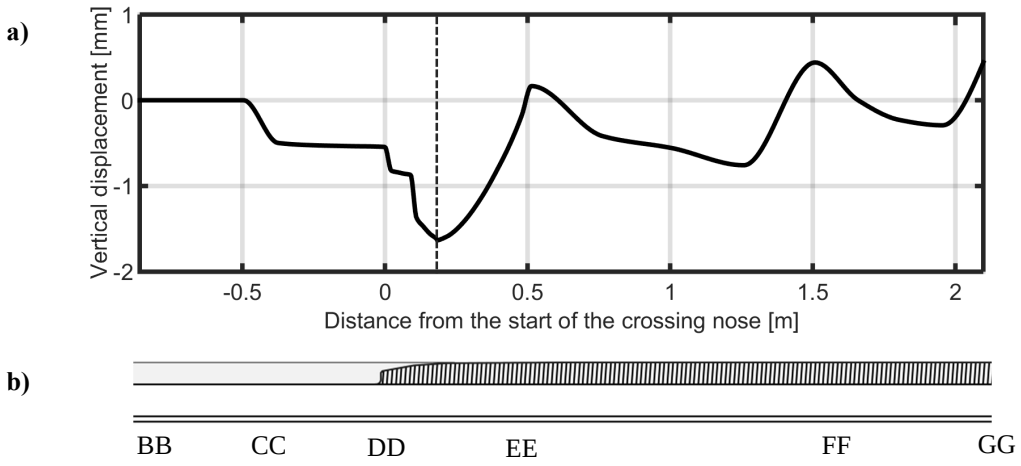

Figure 16: a) Vertical wheel movement along the crossing panel for zero lateral shift of wheelset; b) longitudinal cross section of the crossing panel

In short, it can be summarized that the geometric contact analysis is reliable and efficient enough to extract important contact conditions including initial contact point location, normal contact clearance and the vertical movement of the wheel trajectory. These information's are used as input parameters to build the 3D finite element model as will be explained in the coming section.

3.4. 3D-dynamic finite element contact analysis

A 2D-static analysis as described in the previous section is an insightful tool but is insufficient to analyse a complex problem such as wheel-crossing interaction, since the impact event is in fact a dynamic problem. In order decompose this problem, a 3D finite element model is developed based on the 2D geometric model to perform explicit finite element simulations which enables to assess the arising stress and strain response because of the impact. This section demonstrates the implemented coupling approach and the FE numerical modelling procedure, followed by detailed discussion on the FE simulation results.

3.4.1. Finite element wheel-crossing model description

In order to clearly demonstrate the FE wheel-crossing contact model, a schematic diagram of the dynamic wheel-crossing model is shown in Figure 17a. The mass of the vehicle is a lumped and supported by primary suspension represented by a group of springs and dampers. Also the substructure is modelled according to linear spring and damping elements. The sleepers are substituted with mass elements, and the equivalent spring and damping elements are used to model the rail pad and ballast, see Table 1 for their respective material properties. The locations of the supports (sleepers) are in accordance with the standard design drawings as shown in Figure 9. The coordinate system used here is; X is the lateral direction, Y is the vertical direction and Z is the longitudinal direction, see also Figure 17a.

Table 1: Material properties and operational parameters [23].

Parameters			
Wheel load	= 100 kN	Elastic modulus steel	= 210 GPa
Traction Load	= 25kN	Manganese steel	= 190 GPa
Sleeper mass	= 244 kg	Yield stress	= 480 MPa
Passion's ratio steel	= 0.3	Density of steel	= 7800 kg/m3
Static friction coeff.	= 0.5	Kinetic friction coeff.	= 0.5
Primary stiffness	= 1.15 MN/m	Primary damping	= 2.5 kNs/m
Rail pad stiffness	= 1300 MN/m	Rail pad damping	= 45 kNs/m
Ballast stiffness	= 45 MN/m	Ballast damping	= 32 kNs/m

The actual 3D finite element model is shown in Figure 17b-e. The wheel model developed by Ma [15] and the crossing model developed by the present author are combined in this work to perform dynamic simulations. In order to increase the computational efficiency of the FE solution, only 7.45m of the crossing part is modelled and only half of the wheelset as shown in Figure b-c. The normal rail together with the guard rails are neglected since the lateral movement of the wheel is disabled. The wheel and the crossing models are specifically built to capture the rolling contact stresses in the transition zone of the crossing panel. The operational conditions as well as formulations of the contact conditions are discussed separately in the coming pages.

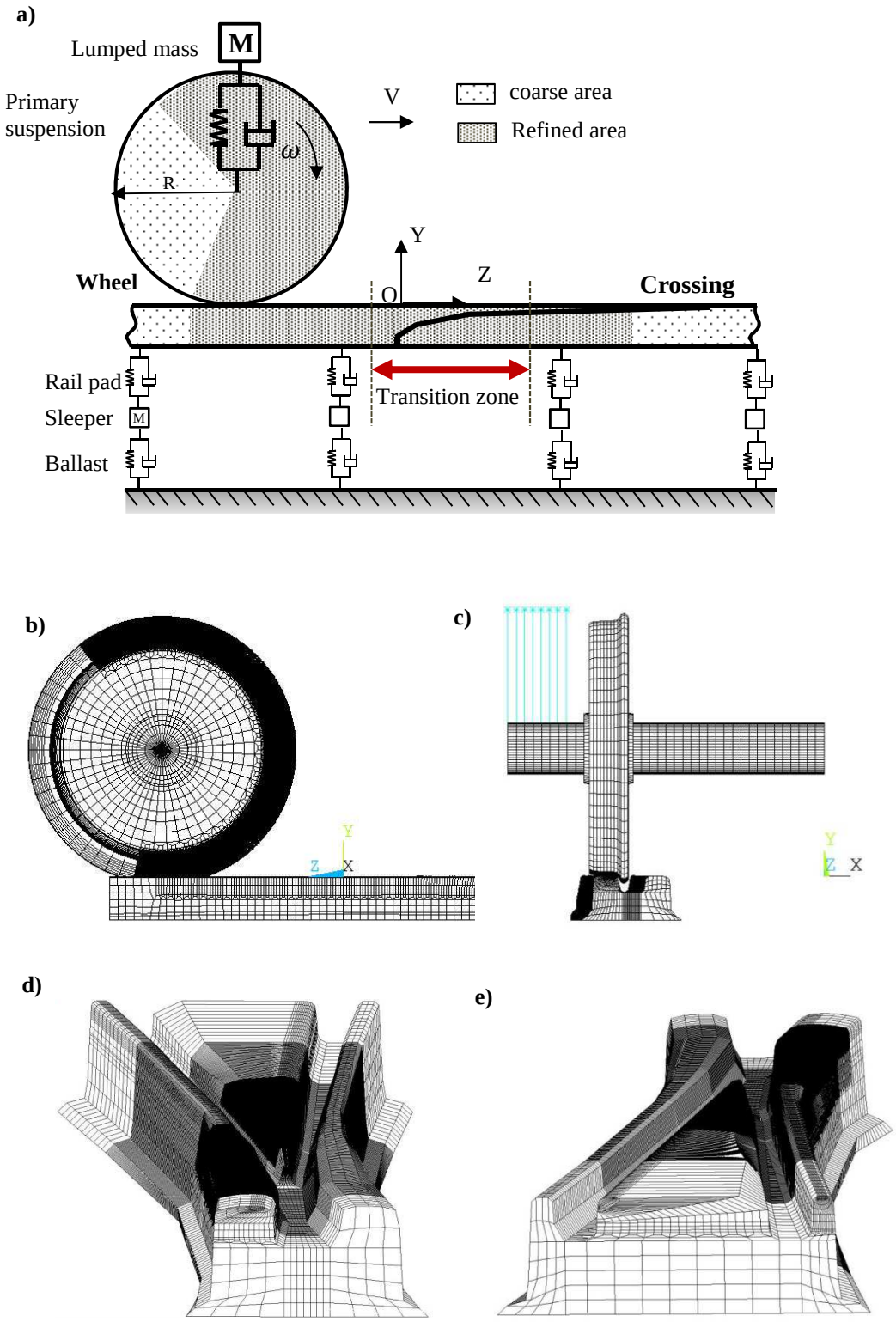

Figure 17: Dynamic FE Wheel-crossing model. a) Schematic diagram of the FE model; b) Side view; c) Front view; d) Facing direction view; e) Trailing direction view.

3.4.2. Finite element meshing process

One of the fundamental parts of solving contact stress problems using finite element method is to locate potential contact areas reliably and efficiently. Furthermore, once the possible contact areas are identified, further refinement has to be done in the vicinity of the stress concentration areas to achieve accurate results. At the same time, using dens mesh will drastically increase the amount of elements thus lead to substantial calculation cost. Therefore, when considering a large model like a crossing panel of 7.45m, it is important to use an efficient refining method to reduce the out-of-contact elements as much as possible. As it already mentioned, the 2D geometric model has been used to pinpoint the potential contact region Prior to the FE modelling. The advantage of this approach is it makes it possible to reduce the amount of fine mesh elements and making sure that the fine mesh is located at the actual place where the wheel and the rail come in contact with each other. If the location of the potential contact area does not match with the actual contact area than the accuracy of the solution cannot be assured

The coupling approach between 2D geometric and the FE model is demonstrated in Figure 18a. The initial contact point locations are highlighted in Figure 18a-b where it can be seen that for this specific case, double point contact occurs which means that the wing rail as well as the crossing nose should be refined.

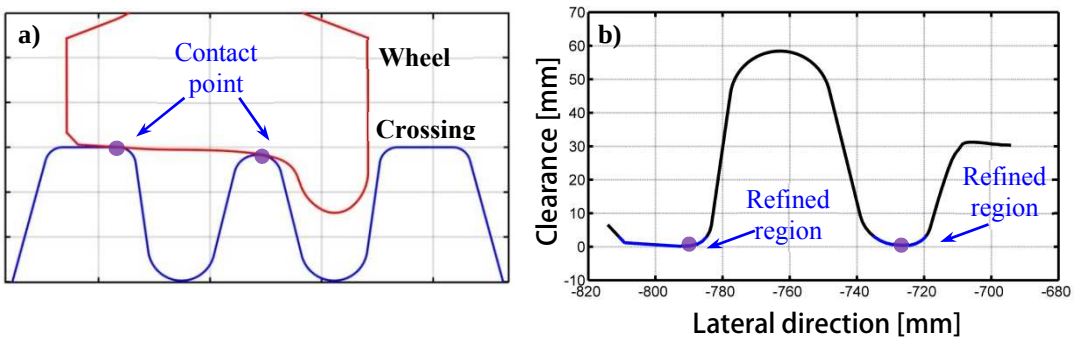

Figure 18: 2D geometric contact simulation. a) Contact point location at zero lateral shift of the wheelset. b) Identifying the refined region based on normal contact gap.

Based on the normal contact clearance, as shown in Figure 18b, the potential contact area can be estimated. It makes sense to assumed that as long as the contact clearance is very small (say from 0mm till 5mm), contact can occur within this range due to the deformation at the contact interface. The exact location of this region is thus important to know so that directed refinement can be made. Since the wheel-crossing interaction at the crossing panel is complex, the process of finding the contact location should be performed for multiple longitudinal cross sections in order to identify the running band of the wheel.

Once the potential contact regions for multiple cross sections are found, the cross sectional data with indication of the contact region is discretized in key points and stored in a text file. In ANSYS program, an APDL script is invoked to import the created key points connecting them using splines, see Figure 19a. When all the cross sections are imported into ANSYS, the solid model is built as shown in Figure 19b.

Based on the indications on the refined regions, a novel adaptive refining technique, as explained in [15], is used to accelerate the meshing process as well as to restrain the calculation expense of the FE model into an acceptable level. Figure 19c-f shows the meshed structure. The wheel and the crossing are modelled according to the same mesh method resulting in a very fine mesh in the contact zone with an element size of 1 mm × 1 mm × 1 mm in the contact region. When using an automatic free mesh without mesh control, the same dens mesh division of the contact region will be enforced on the surrounding elements resulting in dense mesh also in the out-of-contact region. In order to avoid this, transition mapped quadrilateral elements is applied in order to gradually coarsen the mesh, see Figure 19d-e. The crossing panel consists of approximately 450.000 eight-noded hexahedral solid elements and the wheel has 550.000 elements.

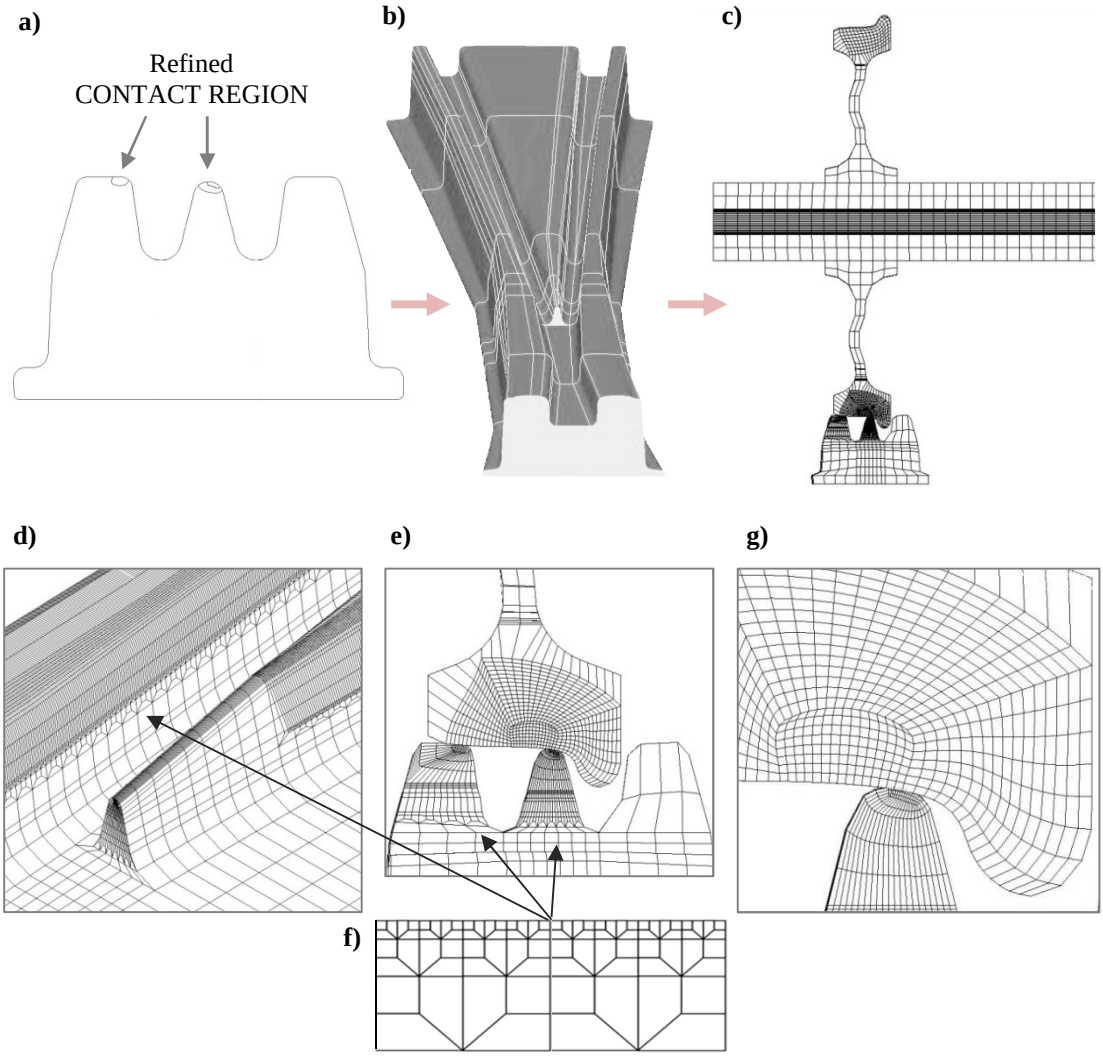

Figure 19: a) Cross section in ANSYS with indication on the contact region; b) FE crossing solid model; c) Lateral cross section of the meshed FE model; d) Close up view of the transition zone; e) Zoom view in to the lateral cross section; f) transition mapped quadrilateral mesh pattern; g) Zoom view nose rail

3.4.3. ANSYS LS DYNA simulation process

The presented FE model is used to simulate the dynamic impact event with the help of ANSYS LS DYNA software package. The in-built feature of the program so called 'implicit-to-explicit sequential solutions' is utilized because it is specifically designed to simulate highly nonlinear transient dynamic events like for our case the wheel impacting on the crossing. Prior to obtaining the time varying behaviour of the FE model, first, a quasi-static structural analysis is performed in which the wheel and rail bodies are brought into contact and the wheel is gradually preloaded, this part will be explained in this subsection. The contact geometry from this analysis is then used as an initial condition for the explicit (dynamic) wheel-crossing rolling process, which will be discussed in the next subsection.

ANSYS - Implicit simulation set-up

In order to capture the impact of the wheel on the crossing, first an initialization step is required. This step called 'implicit analysis' is a quasi-static analysis in which the wheel is placed at the prescribed position on the crossing model and then the complete structure is preloaded with the prescribed wheel load.
Figure 20a-b shows the initial positioning of the wheel on the crossing. For nonlinear geometries, this processes can be critical and complicated, because it is difficult to reach a good compromise between having a large initial contact gap or too much initial penetrations. If either one of these two situations occurs then the implicit solution cannot converge because the two contact pairs (master & slave corresponding to wheel & rail elements) are out of contact. However, using the 2D geometric model, it is possible to calculate the exact relative position of the wheel and the crossing where the initial contact gap is almost set zero (0.0077mm), which in turn, accelerates the calculation process and guarantees a converged solution. See Figure 20c-d for the contact pairs and their relative positioning.

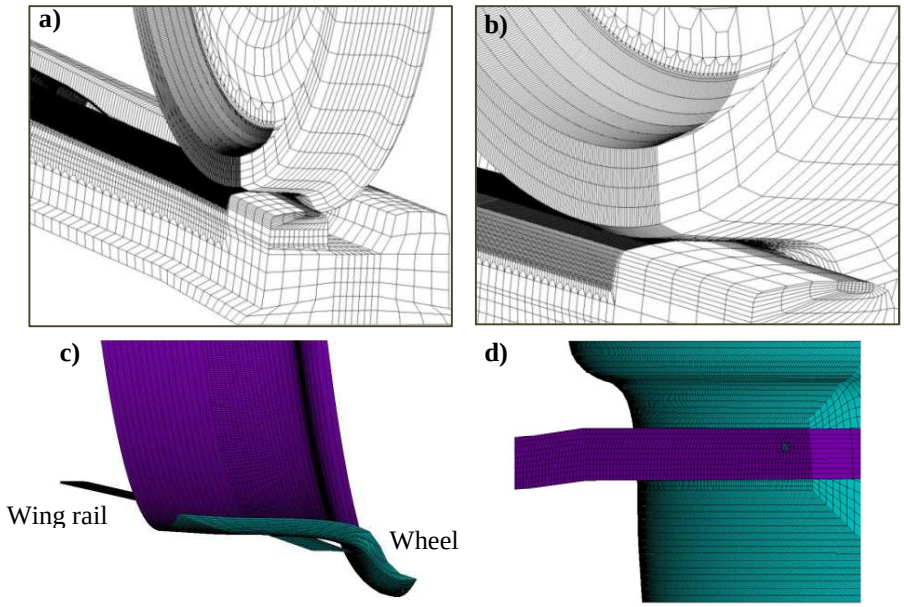

Figure 20: The FE Wheel-crossing model. a) Initial positing of the wheel on the crossing; b) zoom view; c) Contact pairs 3D view; d) Contact pairs plane view

Various algorithms are available in ANSYS which calculates the contact situation. In this work, Augmented Lagrangian algorithm (default option) is used for contact calculations. For the crossing, the (4-node) element CONTA173 is chosen and for the wheel, element TARGE170. The contact forces are calculated though invisible springs which are applied on nodes of the contact pairs as shown in Figure 21. The Augmented Lagrange contact formulation is given by:

$$F_n = k_n \cdot \Delta x_p \tag{1}$$

Where:
F_n = Contact force
k_n = normal spring stiffness
x_p = penetration

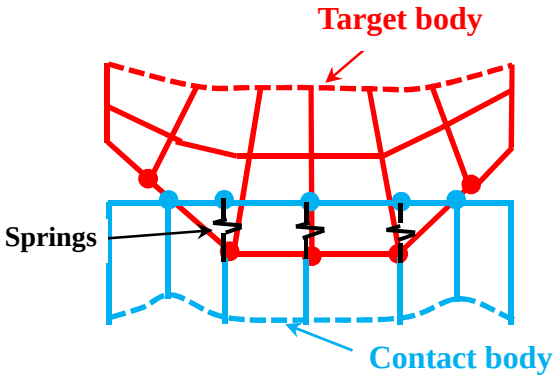

Figure 21: Schematic graph of the contact pair interaction

The higher the contact stiffness, the lower the penetration x_p. Ideally, for an steel on steel contact, infinite k_N is desirable because physical contacting bodies do not interpenetrate, however this is numerically not possible. Moreover, very high spring stiffness requires many iteration to reach converges solution, which in turn, will increase the calculation expense. As long as x_p is very small (in the order of 0.1mm) converged solution can be achieved. Table 2 shows all the parameters used in the implicit analysis.

Table 2. Implicit simulation parameters

Parameters	
Augmented Lagrangian algorithm	Bilinear Isotropic hardening materials
Preload = 100 kN	Quasi-static analysis = 15 load increments
Initial gap = $7.9681*10^{-6}$ m	Maximum penetration = $0.6401005*10^{-6}$ m
Calculation time = 19 hr	Penetration tolerance = $0.1576*10^{-3}$ m
Tangential contact stiffness = $0.4287*10^{15}$ N/m^3	Normal Contact stiffness = $0.20454*10^{16}$ N/m^3

The crossing panel is placed on elastic foundation and the boundary conditions for the most left and right ends are set as:

- **Uz=0** (longitudinal movement of the nodes constraint)
- **Ux & Uy = free** (no constrains in vertical and lateral directions)

Implicit simulation results

At the end of the analysis, the wheel load is completely active and the whole structure is in its deformed state. From Table 2 it can be read that the maximum penetration at the wheel-crossing interface after applying the wheel load is 0.00064 mm, which is negligible small. Figure 22a shows the deformed shape of the structure at the end of the quasi static analysis. The max displacement of 0.702 mm occurred for some nodes on the rail head, directly under the wheel. For the same figure, the maximal vertical displacement (downwards) for a node at the railhead at the left and at the right of the boundaries are also shown. Since the wheel is closer to the left boundary, the displacement at the left boundary (0.108 mm) is larger than at the right end (0.0035mm).

Figure 22b shows the Von Mises Stress (VMS) for the elements at the rail head. It can be observed that the maximum VMS is located well within the refined mesh zone. Figure 22c displays the solution results as continuous contours across element boundaries. Contours are determined by linear interpolation within each element from the nodal values, which are averaged at a node whenever two or more elements connect to the same node. It can be noted that the maximum stress of 540 [MPa] resulting from the applied wheel load of 10t looks reasonable stress state for such a small contact patch [24]. Therefore, it can be noted that simulation results so far are acceptable since it corresponds well with real wheel-rail response.

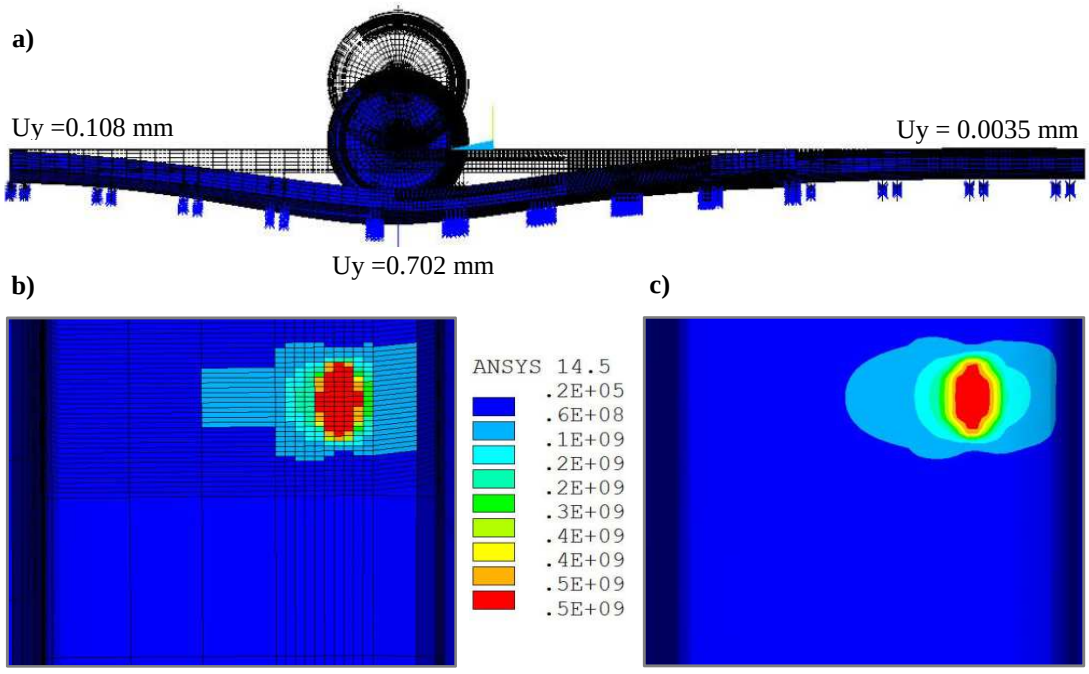

Figure 22: a) deformed structure b) normal stress at rail surface elements; c) interpolated normal stress contours

LS DYNA - explicit simulation set-up

In the implicit analysis, as described in the previous page, the simulation was performed quasi statically, in order to obtain the preloaded and deformed structure. At the end of the simulation, the nodal displacements and rotations are recorded and written in a text file. At the start of the explicit simulation, the written text file is invoked and the nodal displacements are set as initial conditions for the new simulation to start.

In the explicit analysis the wheel is set to roll, either in the facing or trailing direction towards the transition zone which is 1m away from the initial position of the wheel. This distance is needed to achieve stable rolling contact conditions before the impact event takes place. The wheel is set to roll from standing position to a prescribed angular and translational velocity, thereafter continuous traction load is applied on the wheel to maintain its operational velocity. Besides, during the simulation, the yaw motion of the wheelset is disabled since the changes in the wheel set's yaw and roll angles are very small over a short distance.

Figure 23 shows the contact pairs for explicit simulation. It can be seen that for the crossing panel only a small potential contact area, which was already calculated with the 2D geometric model, has been assigned as contact pair. The contact pair for the wheel is relatively large due to the variation of the contact point at the wheel tread. Limiting the contact pair region is desirable since it will decrease the calculation time, however, the potential contact region should encompass the actual contact region otherwise contact forces cannot be calculated.

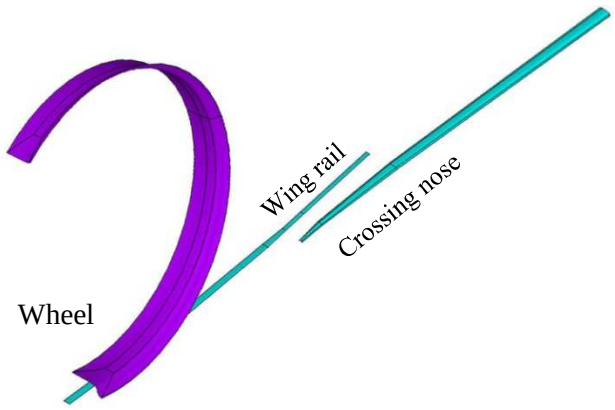

Figure 23: Explicit contact pairs.

The explicit analysis of LS DYNA supports only contact algorithm based on penalty method to calculate the contact properties. The penalty method is based on the same contact formulation as in Eq. (1), however the user has now some control on its numerical values though a scaling factor. The contact stiffness parameter for the penalty method is defined as:

$$k_i = \frac{\alpha \cdot K_i \cdot A_i^2}{Volume} \qquad (2)$$

Where:

k_i = The spring stiffness

K_i = bulk modulus of contacted element,

A_i = area of contact segment

α = penalty factor (0.1 by default)

The spring stiffness can be adjusted through the scaling the penalty factor α. The spring constant is an important parameter that greatly influences the accuracy of the simulation results. Experience has shown that choosing penalty factor α =10 usually gives a good compromise between calculation time and accuracy of the results [15]. Besides, from the contact stiffness relationship, in Eq. (2), it can be observed that the mesh area density has a quadratic influence on the contact stiffness parameter. In this work special care has being taken to make all the contact element of the same size namely 1mm x 1mm x 1mm. This is important because non-uniform distributed mesh size results in varying contact stiffness which can influence the results. The explicit simulation parameters for one specific run are listed in table 3.

Table 3. Explicit simulation parameters

LS-DYNA Simulation set-up			
Penalty method algorithm		Bilinear Isotropic hardening material model	
Automatic surface-to-surface contact		Elastic substructure	
Simulation distance	= 1.7 m	BC at the two ends	Uz = 0/ Ux,Uy =free
Train velocity	= 140 km/h	Mesh size contact region	= $1mm^3$
Wheel load	= 100 kN	Time step size	= $1.8*10^{-4}$ s
Traction load	= 25 kN	Simulation time	= 0.044s
Contact damping	= default	Time steps	= 250 steps
Penalty factor α	= 10 [-]	Calculation time	= 48 hr

3.4.4. FE dynamic simulation results

Using the presented finite element model, explicit simulation is performed according to the procedure described in Section 3.4.5, to calculate the dynamic forces and the stress distribution which are induced due to the wheel-rail frictional rolling contact. This section analyses and explains the obtained results from the wheel running at the crossing nose, taking into account the realistic operational conditions.

Resultant contact forces

After the completion of the dynamic simulation, ANSYS provides data files where the time domain behaviour of each node is registered. MATLAB has been used to organize these data for presentation purposes. The results presented here are for the scenario in which the wheel runs with a constant speed of 140 km/h in the facing direction over the crossing panel. The prescribed loads are 100 kN for the static wheel load and 15 kN for the traction load.

The vertical wheel trajectory is shown in Figure 24a while the resultant contact force along the crossing with respect to rolling distance is shown in Figure 24b. The vertical and the longitudinal contact forces in this figure are of major interest since they are related to the applied axle and traction load. It can be seen that initially the vertical contact force is noisy, this is because the wheel starts to accelerate from a standing position to the prescribed angular and translational velocity. Such sudden acceleration causes unstable wheel motion.
The wheel begins to roll with a local rolling radius of 460 mm and, initially, there is no change in the rolling radius of the wheel. However, at 0.5m before the crossing nose front, the wing rail starts to diverge from the straight path causing a change in the rolling radius of the wheel. From Figure 24a it can be observed that this change in rolling radius induced contact force oscillation between -0.5 and -0.4 m. As the wheel travels further, the contact force oscillation continue to occur due to the discrete support which excites the lumped mass carried on primary suspension.

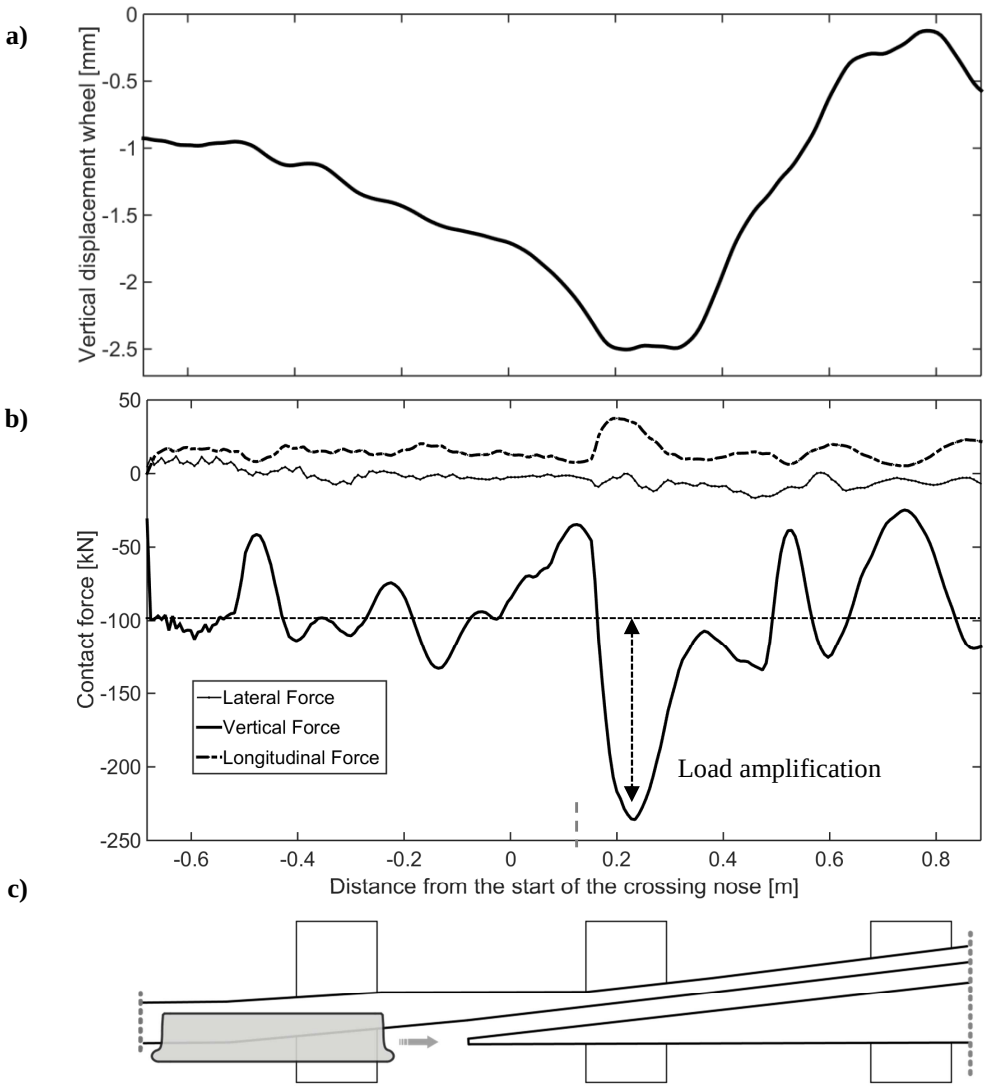

Figure 24: a) time domain contact force w.r.t rolling distance. b) Frequency domain contact force w.r.t rolling distance. c) Top view crossing panel

As the wheel makes the transition from the wing rail to the crossing nose, high impact forces can be observed at 0.223 m with almost 2.5 times the applied static wheel load. This phenomenon corresponds well with the literature research [17, 25]. From Figure 24a it can be seen that in the transition zone the wheel drops. Moreover, it can be noticed that during further onward movement, the wheel movement suddenly reverse which corresponds to the sudden strikes the crossing nose while moving further on the crossing nose. Such a sudden rise of the wheel at the nose within a very short time space causes severe vertical accelerations in the wheel axles. Consequently, it results in high vertical reaction force and longitudinal force due to the severe rubbing of crossing nose surface. More discussion and suggestions on how to improve the vertical wheel movement will be presented in Section 5.3.

Surface stress distribution during impact

As it was seen from the previous figure, an impact event is associated with large and abrupt changes in the movement of the contacting bodies which results in amplification of contact forces. Such high forces and vibration of the wheel within a very short time cause stress wave propagation through the system which in turn causes local elastic and plastic deformations at the contact zone.
Figure 25 illustrates the running band of the wheel along the crossing panel. The most governing and critical part is the transition zone where extreme values for the contact stresses are recorded. In order to investigate this, Figure 26 shows the Von Mises stress distribution at the contact patch during the impact event. Before the transition (Figure 26a), the contact patch runs only on the wing rail and the residual stresses are dragging behind in the running band. At the start of the transition zone (Figure 26b), double contact occurs both on the wing rail and the crossing nose. During the further onward moving of the contact patch (Figure 26c-d), the stresses at the wing rail gradually decrease, while the one on the crossing nose rapidly increase. At the end of the transition zone (Figure 26d), the wheel load has been completely transferred to the crossing nose. At this critical time moment the highest stress level up to 1240 MPa was recorded. Moreover, it can be observed from the stress dispersion on at the right side of the crossing that the stresses waves penetrate also into the subsurface material. A detailed subsurface stress analysis is presented in the next subsection.

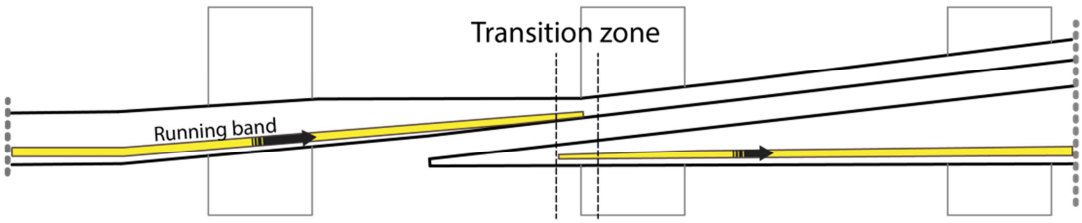

Figure 25: illustration of the running band

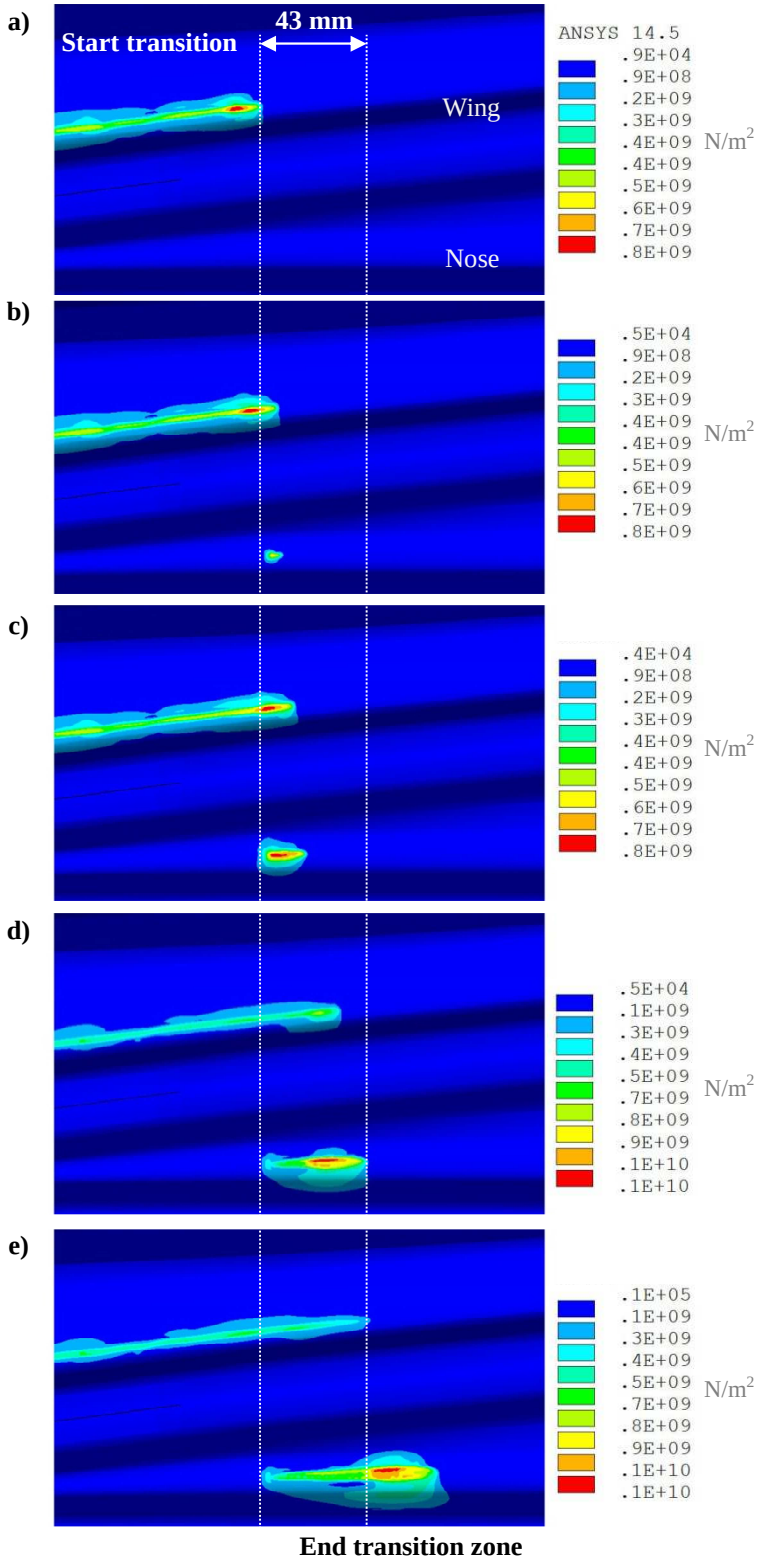

Figure 26: Von misses stress distribution at the transition zone from the explicit 3D FE analysis. a) Prior to the transition process. Only single point contact on the wing rail. b) Start of the transition process. Double point contact on the wing rail and the crossing nose; c-d) During the transition process. Contact on the wing rail gradually vanishes while on the crossing nose increases; e) End of the transition process. Only single point contact on the crossing nose.

Subsurface stress distribution during impact

In the crossing nose often severe damage in the form of wear, plastification and cracks is observed. The high impact loads on the crossing nose does not only affect the surface material but it penetrates into the subsurface. Here, subsurface analysis is performed to reveal the stress state in the subsurface. The most critical time moment when the distribution of the Von-Mises stress reaches peak value is at 223 mm from the front of the crossing nose as shown in Figure 27a-d. At this moment maximum Von Mises stress of 1240 MPa was recorded.

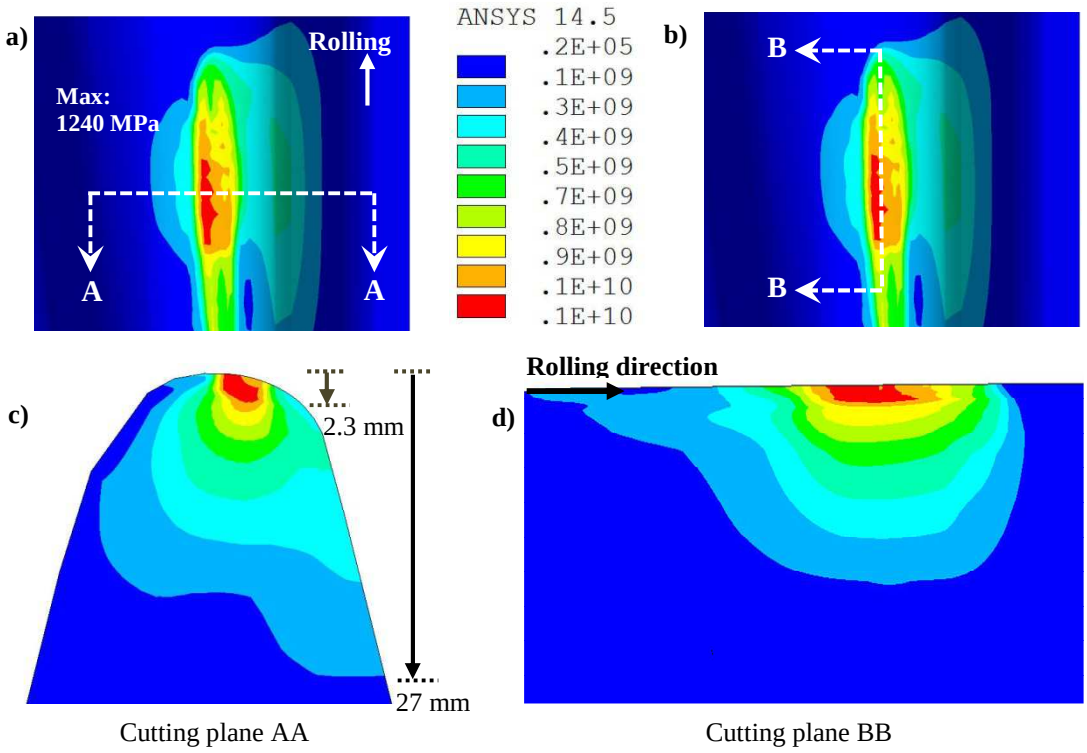

Figure 27. Bilinear (plastic) materials. Von Mises Stress distribution at 223 mm from the crossing nose front. a) Lateral cutting plane AA; b) Longitudinal cutting plane BB; c) Von-Mises stress at lateral cutting plane AA; d) Von-Mises stress at longitudinal cutting plane BB.

It can be seen that, although plastic material model is used, the maximum stress of 1240 MPa is far above the yield limit of wheel and rail materials. Such a high stress concentration is possible because of the relatively small size of the contact patch. Besides, from Figure 27c-d it can be seen the state of stress produced by rolling contact is concentrated in rather a small volume of material. Due to this, plastification of the surface material is likely to occur because of the intense plastic strain. Furthermore, Figures 28 & 29 show the vertical normal stress and longitudinal shear stress respectively. Due to the impact on the crossing nose, the prescribed wheel load of 10t is amplified with a maximum contact pressure of approximately 2000 MPa, acting in the contact nodes. As the wheel is rolling from left to right, it can be seen that compressive shear pressure at the rear of the contact patch is created and tensile shear pressure in front of the contact patch.

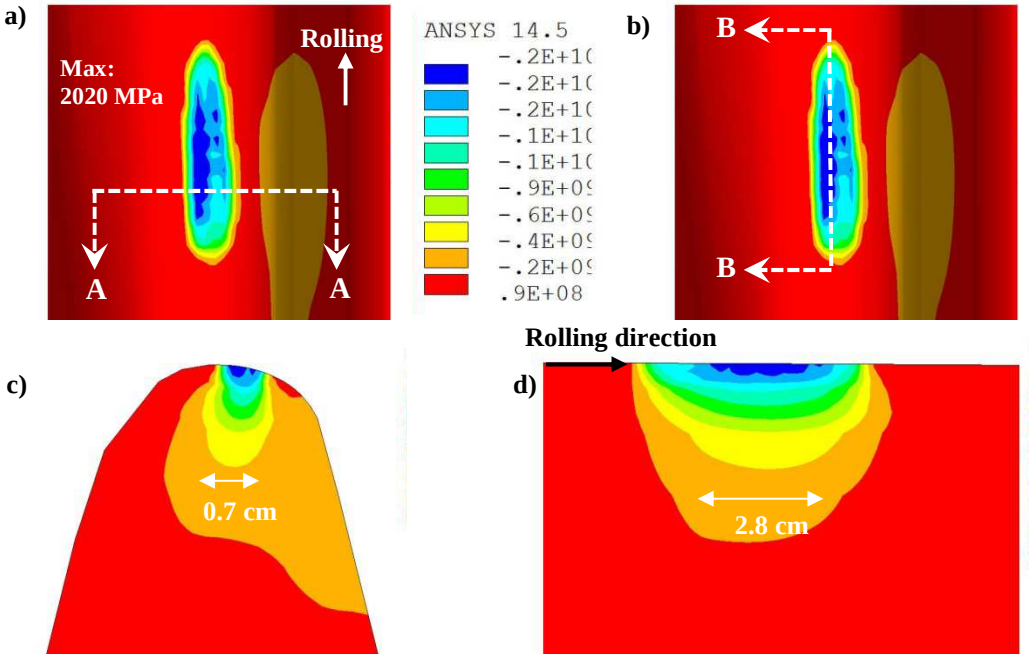

Cutting plane AA Cutting plane BB

Figure 28. Bilinear (plastic) materials. Normal stress distribution at 223 mm from the crossing nose front. a) Lateral cutting plane BB; b) Longitudinal cutting plane AA; c) Von-Mises stress on BB Cutting plane; d) Von-Mises stress on AA Cutting plane.

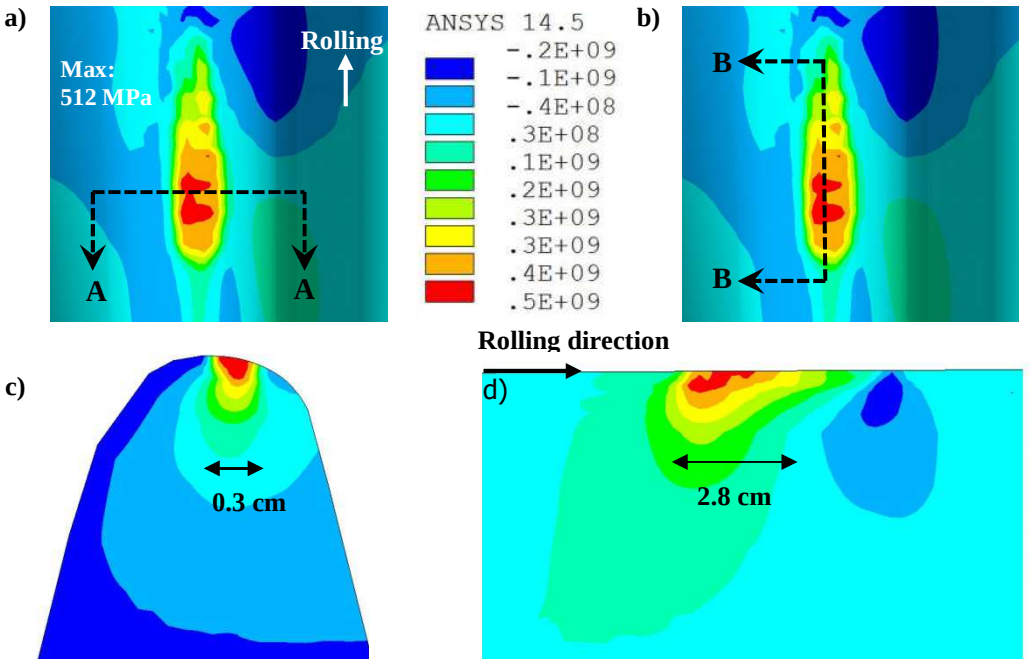

Cutting plane AA Cutting plane BB

Figure 29. Bilinear (plastic) materials. Shear stress distribution at 223 mm from the crossing nose front. a) Lateral cutting plane BB; b) Longitudinal cutting plane AA; c) Von-Mises stress on BB Cutting plane; d) Von-Mises stress on AA Cutting plane.

4.

Verification & validation

The results obtained from the FE model, as shown in the previous section, do provided realistic and reasonable prediction of the physical reality. However, it should be assessed carefully because although FE method is a reliable and a powerful technique, it contains many unknown and uncertain parameters which can influence the calculation results. Therefore, it is necessary to verify and validate the developed models with additional studies and the field experiments. In this section, first, the boundary conditions and the numerical stability of the model are discussed. Thereafter, the calculation results from the 2D geometric model and the FE model are verified with each other. Furthermore, the calculation results of the FE model are validated against field measurements to see how close the FE model simulates the reality.

4.1. Influence of boundary conditions

The main problem of FE model with a finite length is that boundaries may introduce undesirable effects in studying the response to a moving load. This section investigates the influence of the boundary conditions on the numerical stability of the solution. Three FE models has been built, with different lengths of the crossing panel as shown in Figure 30.

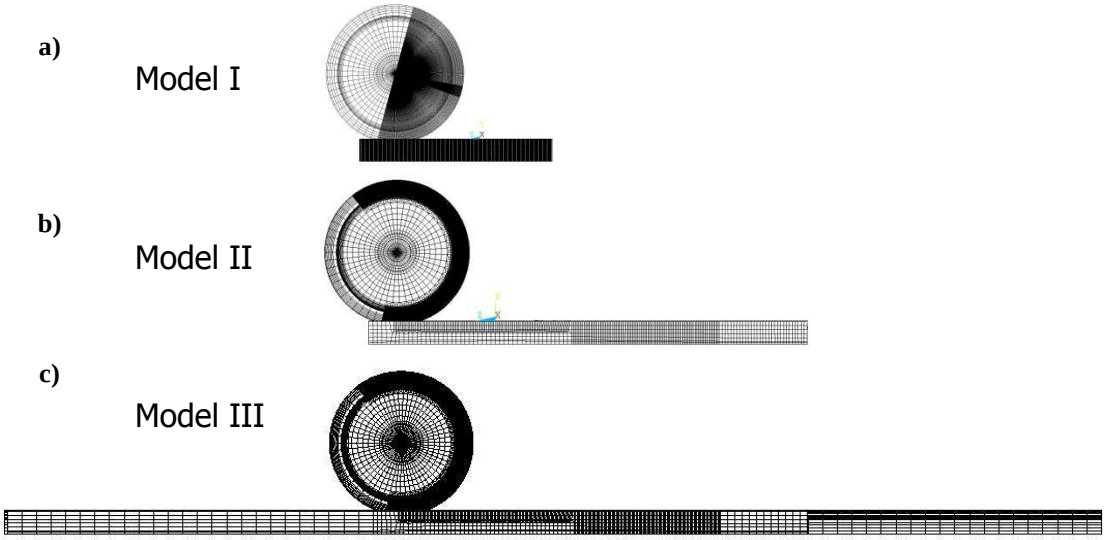

Figure 30. The FE models. a) Initial model; b) prolonged model; c) final model

Some characteristic information about these three models are shown in Table 4. Model III is more than six times larger than model I, due to a novel mesh technique the amount of elements has been significantly reduced. Besides, from this table it can be seen that as the model becomes longer, the vertical displacement of the two boundaries converge to zero. This is important because it indicates that their influence on the numerical solution is decreasing.

Table 4. Summary of the presented results

Model	Total length model [m]	Amount of supports	Amount of elements	Displacement. left end [mm]	Displacement. right end [mm]
I	1.2	3	450.000	4	2
II	3	6	380.000	2	0.5
III	7.45	13	391.145	0.108	0.0035

This can be also confirmed from Figure 31 in which the contact force distribution for the three models is shown. Here, it can be observed that Model I has a shorter running distance and large contact force oscillations compared with Model II & III. Furthermore, it can be seen that as the length of the FE model increases, the numerical solution is converging. This is clearly apparent from the impact event at 0.2m after the crossing nose front. Based on this, it can be concluded the FE model provide acceptable results for studying the impact event.

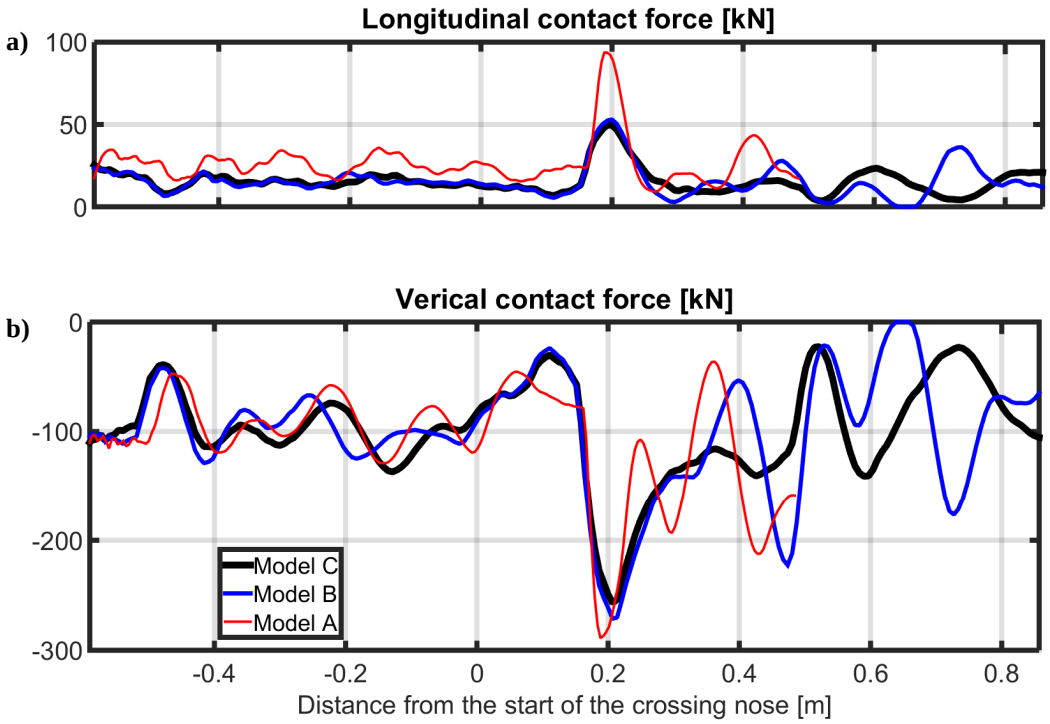

Figure 31. Contact force comparison for the three models. a) Shear force; b) Normal force.

4.2. Verification: 2D geometric model vs. FE model.

A comparison of the vertical wheel trajectory calculated with the 2D geometric and the FE model is shown in Figure 32. It should be mentioned that the FE model considers elastic support and plastic material behaviour whereas the 2D geometric model does not include substructure and the bodies are modelled as rigid. Due to this difference, it can be observed that the vertical wheel trajectory from the FE calculation has an initial settlement of 1mm contrary to the geometric model where the displacement zero at the beginning. Besides, the abrupt changes in the vertical trajectory of the wheel which is clear from the 2D geometric model, has been made more smooth and shallow in the FE model. A good match is achieved at the deepest point of the vertical wheel trajectory at 0.2m. Thus, it can be concluded that although there are some minor differences between the calculation results of the two models, in general the results do show a good agreement.

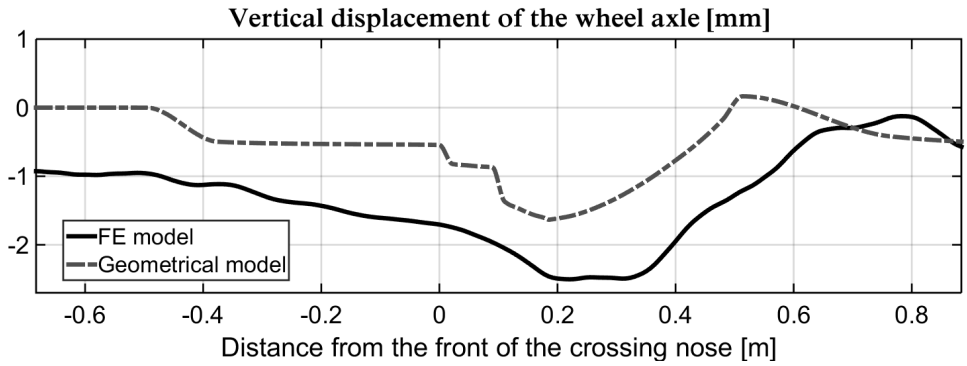

Figure 32: vertical wheel trajectory calculated with the 2D geometric and the FE model.

4.3. Visual observation of the transition zone

Field observation is another important reference to check the precision of the calculation results. In this regard, the transition zone measured from the field is verified with calculation results of the geometric and FE model. Figure 33a-b shows the measured distance of the transition zone from the field and the predicted distance according to the two models. From the measurement it can be seen the initial stage of the transition process starts at 180mm away from the front of the crossing nose and the whole transition distance is approximately 170mm long.

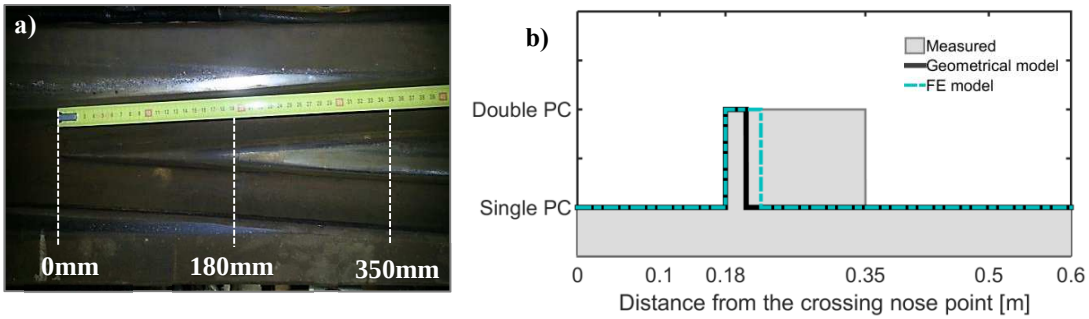

Figure 33: a) Transition distance measured from the field; b)Transition zone comparison

From Figure 33b it is clear that the initial stage of the transition is estimated very well while the transition zone ends to early compared with the field measurement. The transition distance estimated by the geometric model is 25mm and 43mm according to the FE model. Thus, it can be concluded that the 2D geometric analysis and the 3D FE results shown a good agreement in estimating the start of the transition zone, however, the total transition distance from the field measurements seems to be longer than the calculated ones. This is logical because the calculations are based on standard wheel and track profiles and only zero lateral shift of the wheelset is considered. However, in practice, different lateral shift of the wheelset, worn wheel/rail profiles and vertical stiffness of the track can influence the contact point distribution and thus the transition distance.

4.4. Verification against the crossing nose accelerations

This section provides verification of the FE model against field measurements. The Elektronische System Analyse Herzstijckbereich - Mobil (ESAH-M) was used to capture the dynamic acceleration of a particular crossing in the Dutch railway network. The sensor which detects the accelerations were mounted on the side of the crossing at 300 mm from the crossing nose front as shown in Figure 34a. The accelerations recorded at this location are compared with the time history of the nodes located at the same place in the FE model, see Figure 34b. The field measurement data as well as the acceleration of the selected FE node are shown in Figure 34c. The data shown here are only the vertical acceleration due to the passing of the first wheelset which enters the crossing. Besides, the measured data has been selected for the velocities of more or less 140 km/h in order to ensure that the operational conditions are similar to the one in the FE model. The data of ten separate measurements has been plotted in Figure 34c.

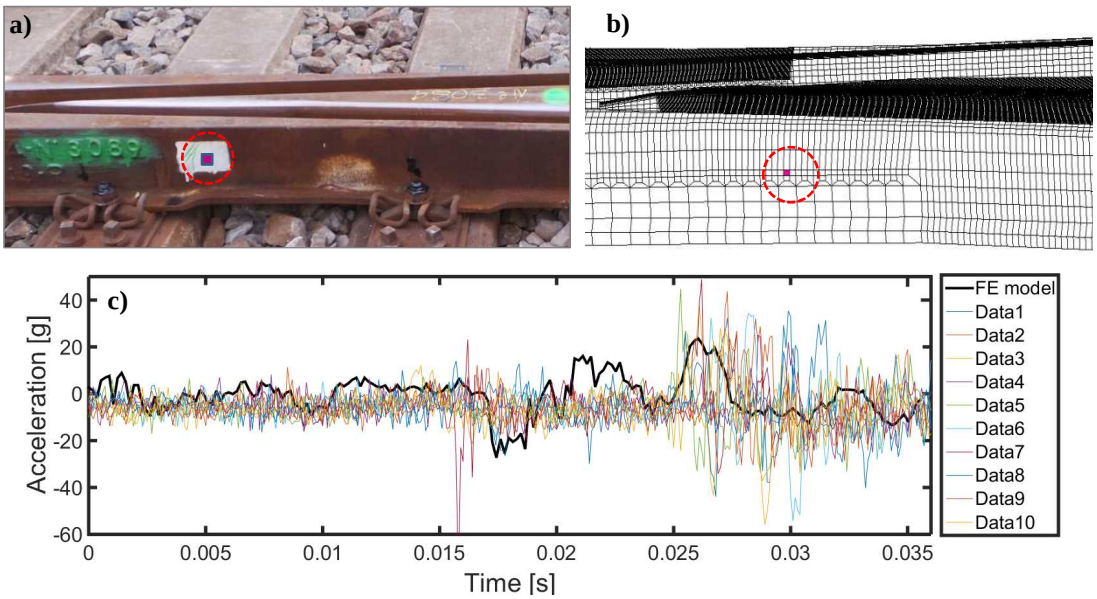

Figure 34: a) Location of the acceleration sensor at the field; b) The node where the acceleration response is captured; c) Comparison of the accelerations from the ESAH-M device and FE model.

A first glance at this figure shows that the highest accelerations occur in the range from -60g to 40g. Such peak acceleration may correspond to an impact on the crossing nose but the location of the impact is varying for the most of the measured data. The main reason for this could be attributed to the fact that at the field the crossing nose is approached by all kind of train with varying wheel loads, wheel profiles and some of them with wheel defects. All of this can influence the magnitude and the location of the impact.

In order to have a better comparison, one particular case has been selected and plotted together with the data from the FE model in Figure 35a. From this figure it can be noted that prior to the impact, the acceleration magnitude is comparable however, at the impact moment, the measured accelerations are significantly higher. The difference in response can be caused of the wheel load at the field which may deviate too much from what it has been assumed in the FE model. Moreover, it can also be attributed to difference of the substructure and the primary suspension properties.

Besides, it can be observed that the ESAH-M measurements has more oscillations than the FE model. In order to study these oscillations more closely, the vibration are separated from each other by Fast Fourier Transformation (FFT) analysis as shown in Figure 35b. Comparing the two signals it becomes clear that ESAH-M measurement consists of high frequency oscillation whereas the accelerations from the FE model operate with low frequency oscillation. This can be explained by the fact the crossing panel was modelled as a solid model whereas at the field a hollow crossing was used which means that the mass and inertia properties of the compared crossing are not the same.

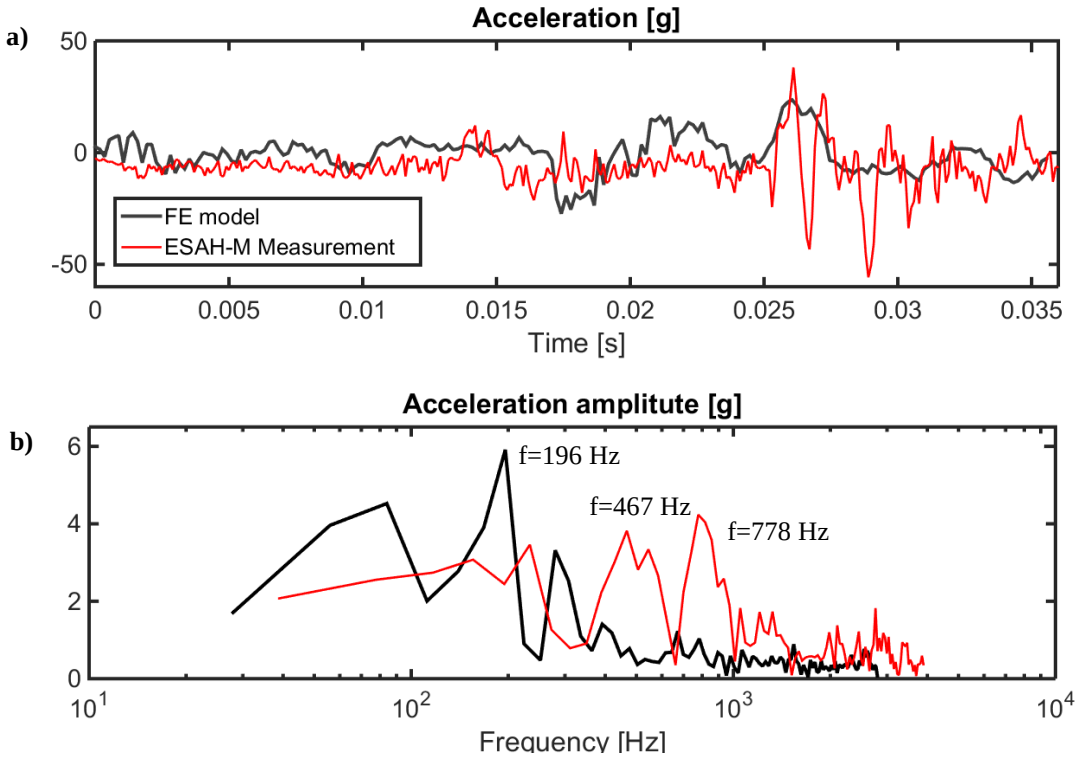

Figure 35: Measured accelerations from the ESAH-M device and the FE model. a) Comparison of accelerations in the time domain; b) Comparison of accelerations in the frequency domain

4.5. Verification against the axle box acceleration

Whereas, in the previous page the vibrations of the crossing for the moving wheel was analysed, here, the accelerations of the wheel itself is analysed and compared with field experiment. The measurements are recorded with The Axle Box Acceleration (ABA) device which measures the accelerations of the wheel axle in a real vehicle-track system. The measured vertical acceleration as well as the time history response of the FE model is shown in Figure 36a. At the moment of impact at t=0.0305 s, the amplitude of the measured acceleration matches very well with the accelerations from the FE model. Also at other time moments, the compared accelerations have some similarities. Moreover, the trend of impacting and stabilization of the vibrations show a good correlation between the two signals. However, the measured signal has more frequent oscillations than the signal of the FE model. This can be confirmed from the signal analysis in the frequency domain as shown in Figure 36b. From this graph it is clear that the FE model vibrations contain vibrations within the frequency band of 47Hz to 230Hz whereas, the measured signal contains predominantly high frequency of 530 Hz.
Therefore, it can be concluded that the FE model and the measurements have some conformities as well as discrepancies. The waveform of the two signals are comparable whereas frequency range of the signals are different. The fact that in the FE model only one wheel is considered and no secondary suspension is included, could be the main reason behind the mismatch of the vibrations.

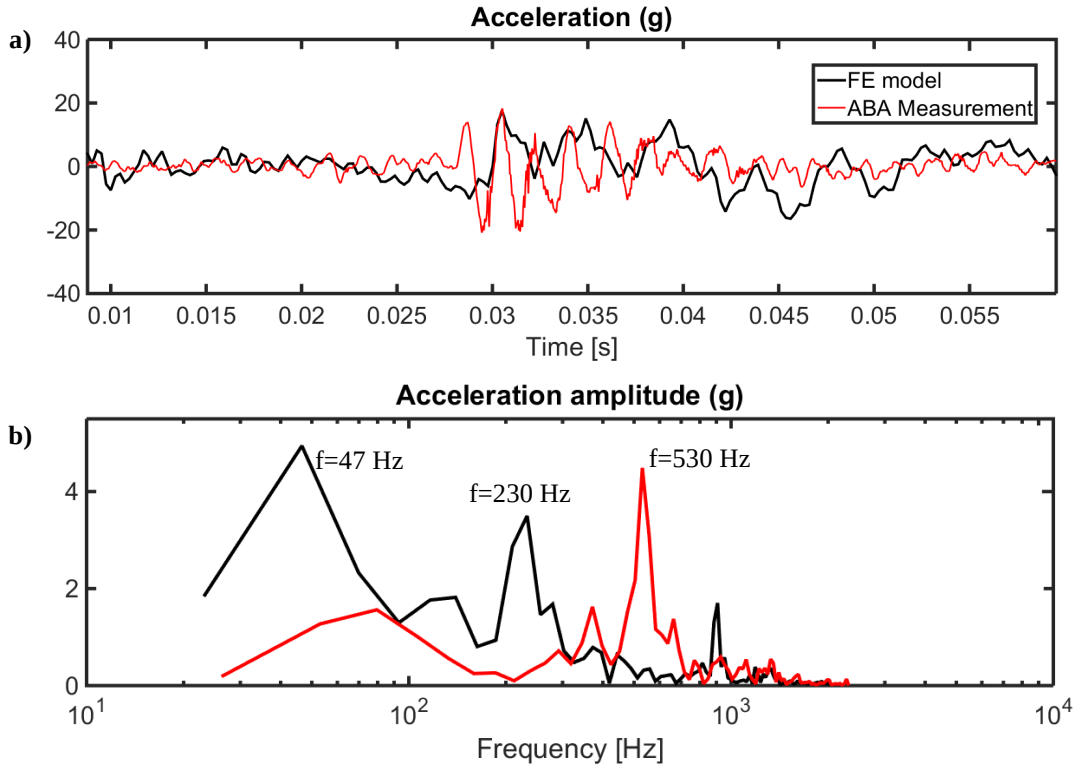

Figure 36: Measured accelerations from the ABA device and the FE model. a) Comparison of accelerations in the time domain; b) Comparison of accelerations in the frequency domain

5.

Parametric study

From the previous section it was seen that developed FE model shows acceptable results compared with the field experiments. Since the FE model has been verified, a parametric study is carried out to investigate the effect of some influential parameters on the contact forces and the local stresses. Such a parametric study does not only provide an improved understanding of the different aspects of railway engineering but it also examines the capability and the flexibility of the FE model under different operational conditions.
In the coming subsections, additional simulations are carried out to study the effects of the impact forces for different material models, vertical substructure stiffness variation, crossing design shape modification and facing/trailing operations.

5.1. Elastic vs plastic materials

As discussed in Section 3.4, due to the impact loads on a rather small contact area, contact stresses can be more than four times beyond the elastic limit of steel. Utilizing linear material properties may raise doubts in the assessment of the structural response. In order to investigate this, a comparison between elastic and plastic material properties are provided in this section to assess the distribution of contact forces and stresses.
As discussed in Section 2, Multibody System (MBS) and Finite Element Method (FEM) are widely used for studies of contact mechanics, considering elastic as well as plastic material contact bodies. Almost all MBS programs incorporate linear elastic material properties whereas in FEM a variety of material models are available to choose from. The advantage of using MBS is that calculation time is extremely fast because it is based on simplified algorithms to calculate contact properties. Contrary to MBS, in FEM it is possible to take into account local deformations occurring at the wheel-rail interface resulting in more accurate predictions of rolling contact forces and stresses. This consideration becomes more and more important when dealing with high stress concentrations, wear and fracture investigations.

5.1.1. Contact force and stress state comparison

Two cases are investigated in this regard to analyse the discrepancies and conformities between these different methods. One, in which wheel and rail are assigned to have linear materials and the second with bilinear plastic materials. Figure 37a shows the stress-strain diagram for the material models incorporated in ANSYS. From this figure one can see that the elastic material model has no yield limit which means that stress can continue to grow along the same slope. In this case the induced stresses do not affect the materials in the sense that it can fully recover its original shape upon unloading. However in reality loading steel above the yield limit will result in non-recoverable plastic strain. This behaviour has been taken into account in the bilinear plastic material model. It shows an initial linear elastic part and an additional hardening (plastic) behaviour.

Figure 37b-c shows the vertical contact force for the two cases. From this figure it can be noted that the differences are not so big. For the case of bilinear material model, the magnitude of the impact force has been reduced. This can be attributed to the fact that when using plastic materials, stress levels beyond the yield limit results in local permanent deformation at the contact patch which results in larger contact area. Due to the redistribution of stresses over a larger contact area obviously, the stresses are lowered as well as the contact forces.

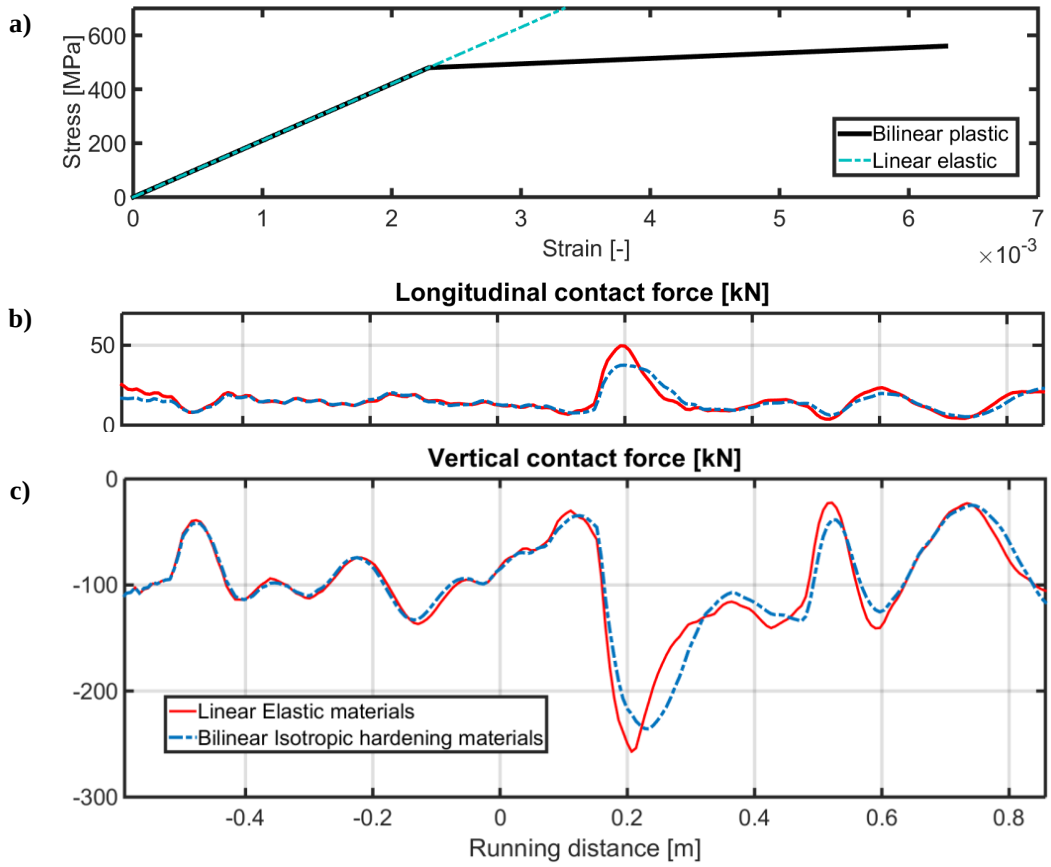

Figure 37. a) Stress-strain curve used in the simulations; b-c) Contact forces according to elastic and plastic materials

The increased contact area for plastic material model can be conformed from the 3D normal pressure distribution shown in Figure 38a & 39a for a critical time moment where highest contact stresses were recorded. The magnitude of the maximum normal pressure, when using plastic materials is reduced up to 40% compared with elastic materials. Besides, from the contour plot in Figure 38b & 39b it can be observed that the contact patch has more or less an elliptical shape in both cases. However, the width contact patch has been increases almost two times when using the plastic materials. Although the size of the contact patch looks quite small it is reasonable compared with real life.

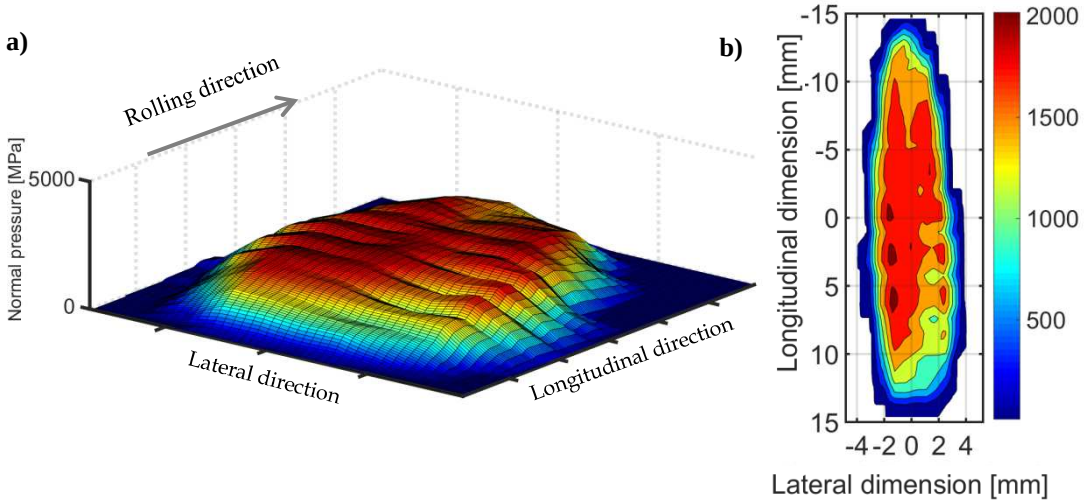

Figure 38. Bilinear (plastic) materials. Surface normal pressure distribution at 223 mm from the crossing nose front. a) 3D shaded surface plot; b) 2D Contour plot;

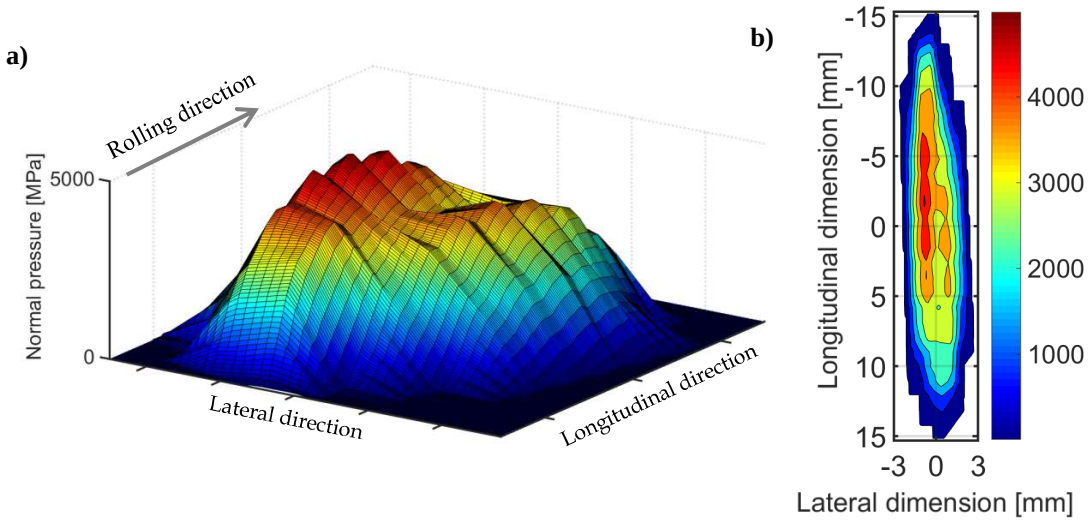

Figure 39. Linear (elastic) materials. Surface normal pressure distribution at 223 mm from the crossing nose front. a) 3D shaded surface plot; b) 2D Contour plot;

The tangential force divided by the contact area gives the shear stress distribution over the contact area, as shown in the Figure 40 & 41. It is captured for the same time moment as for the normal contact pressure. For both cases, the highest shear stress takes place at the rare of the contact patch. Again, it was found that the shear stress using plastic materials was 52% lower compared with elastic case. Besides, comparing the contour plots, the shape of the contact patch for the two cases seems to be significantly different but the location of the peaks are comparable.

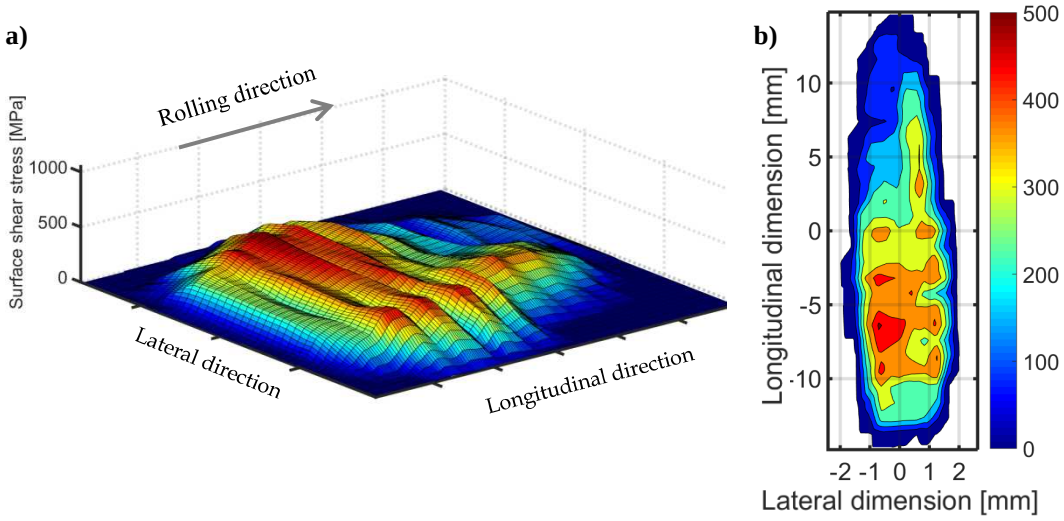

Figure 40. Bilinear (plastic) materials. Surface shear pressure distribution at 223 mm from the crossing nose front. a) 3D shaded surface plot; b) 2D Contour plot;

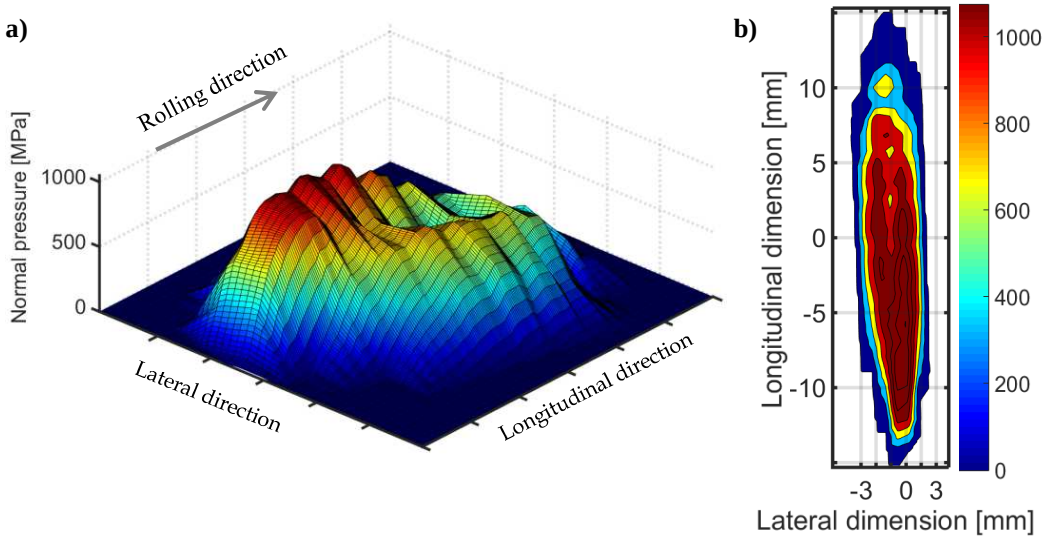

Figure 41. Linear (plastic) materials. Surface shear pressure distribution at 223 mm from the crossing nose front. a) 3D shaded surface plot; b) 2D Contour plot;

5.1.2. Slip-stick region

As discussed in Section 2.1, when the magnitude of the shear stress is smaller than the Coulumb friction law, a sticking state occurs at the contact patch. Alternatively, if the shear stress is larger than the Coulumb friction law then relative sliding takes place which is denoted as micro-slip. Applying this for every node at the contact patch allows us to plot the contact patch divided into slip and stick region as shown in Figure 42 [26]. It can be observed that stick region appears at the leading edge of the contact zone, while the micro-slip zone covers the remaining area of the contact patch. This is corresponds very well with the traction curve shown in Figure 3 where the contact patch in the linear part of the line is governed by partially slip and stick conditions. From the figure below, it is observed that for plastic material properties, the stick region has been relatively increased. Besides, the stick region for plastic case is focused at the top left of the contact patch contrary to the elastic case where the stick region mostly appears at top right of the contact patch.

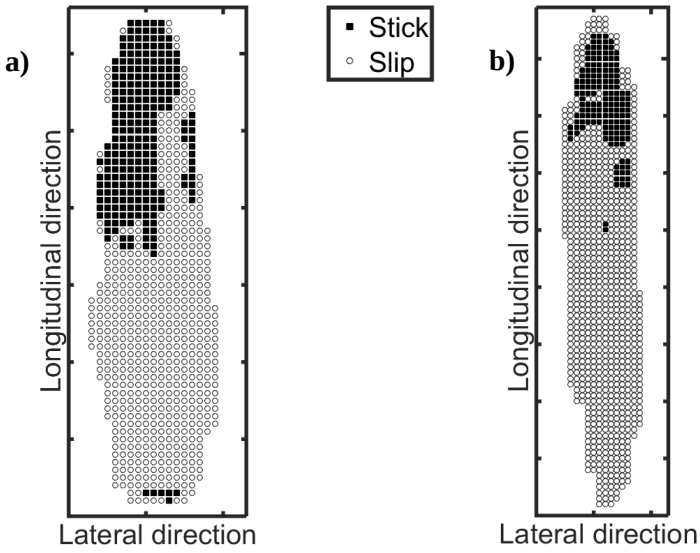

Figure 42. Slip-stick region at the contact patch at 223 mm from the crossing nose front. a) Plastic materials. b) Elastic materials

In short it can be concluded that when comparing the contact forces for plastic and elastic case the difference is not so great. However the magnitude of stresses for these two cases vary greatly. Table 5 shows a summary of the presented results. These results show the importance of using plastic calculations for studies of contact stresses for impact events otherwise the stresses will be completely over predicted.

Table 5. Summary of the presented results

Case	Max. Fy [kN]	Major axis [mm]	Minor axis [mm]	Max. normal pressure [MPa]	Max shear pressure [MPa]
Plastic	212	28 [mm]	7.2 [mm]	2020 [MPa]	512 [MPa]
Elastic	257	27 [mm]	4.2 [mm]	5085 [MPa]	1043 [MPa]

5.2. Vertical substructure stiffness variation

A railway structure can be roughly divided into superstructure and substructure. The superstructure consists of rails, fastening system and sleepers, while the substructure consists of ballast, embankment fill and subsoil. The rapid degradation of the track geometry and generation of impact loads are often linked to poor substructure conditions [27]. In this section, a parametric study is carried out to investigate which combination of soft and stiff substructure stiffness properties in the longitudinal direction of the crossing panel can mitigate the impact loads on the crossing nose. This problem has been extensively investigated in the past using MBS simulations [25, 28], however in this study numerical simulations are performed based on FE wheel-track model which enables to predict the impact forces more accurately.

5.2.1. Case studies

As already mentioned, one of the main cause behind the amplification of wheel loads can be ascribed to irregular (track) support stiffness. It is known that unbounded materials like soil and ballast are inhomogeneous which results in non-uniform substructure stiffness but also the superstructure stiffness is in the case of crossing panel non-uniform due to its the varying moment of inertia [29]. The variation of the support stiffness results in irregular and high accelerations in the wheel axle and thus generating high dynamic loads on the crossing nose.
Figure 43 shows a schematic diagram of the super and substructure of the FE model. The crossing panel is carried by a series of discrete supports ranging from S1 to S13. The support components like rail pads, sleepers and ballast are represented as springs, dampers, and masses elements, whose parameters can be varied independently of each other so that track parameters may arbitrarily vary in the longitudinal direction. Seven additional simulations are carried out in which for every case study (Case A to F) the stiffness parameters are adjusted for some of the supports.

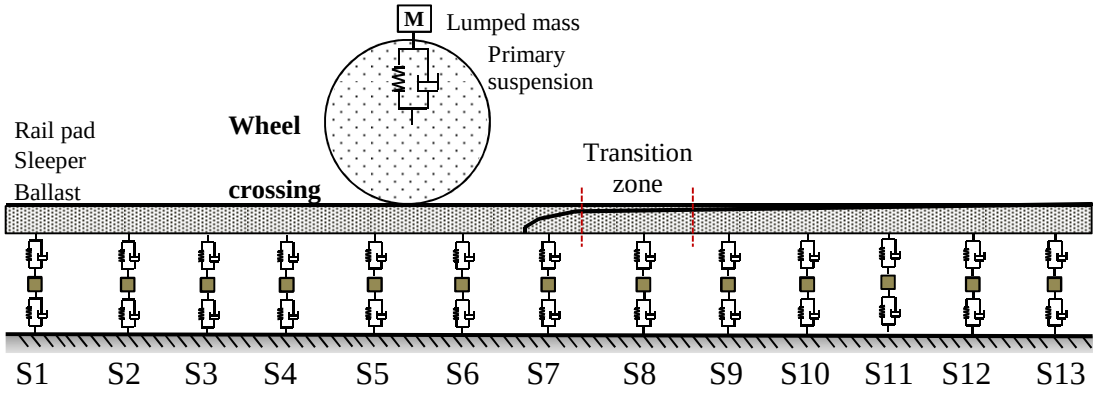

Figure 43. Schematic diagram of the FE model with indication of the substructure numbers.

Table 6 shows adjusted stiffness parameters for the case studies A to F with respect to the reference case, see Table 1 for their respective values. in this parametric study, the absolute values of the stiffness parameters are not so important since these numerical values are meaningless in practise, where it is very difficult to achieve the exact numerical value for the subgrade. However, what is important for this study is the order to the values and the stiffness combinations for the supports.

Table 6. Stiffness parameters for the study case A to G

CASE	Support Nr	Rail pad stiffness	Ballast stiffness	Sleeper mass
Case A	S7 only	100 times lower		
Case B	S7 only		10 times lower	
Case C	S7 only	100 times lower	10 times lower	
Case D	S7 only	100 times lower	10 times lower	2 times lower
Case E	S6 & S8	100 times lower	10 times lower	2 times lower
Case F	S1 to S13	100 times lower	10 times lower	2 times lower

5.2.2. Results and discussion

Figure 44a-b shows the longitudinal and the vertical contact forces for all the case studies. Many of the lines are overlapped in this figure which means that some case studies had limit influence on the contact force distribution. Most notable here is Case E which is the most favourable case in which the transition zone supports (S6, S7 and S8) are made relatively softer than their neighbouring supports. Contrary to this, the most unfavourable situation is Case F in which all the supports were made softer uniformly. Therefore, it can be concluded that longitudinal the position of the supports along the crossing panel as well as its relative stiffness compared with its neighbouring supports has significant effect on the magnitude of the contact forces.

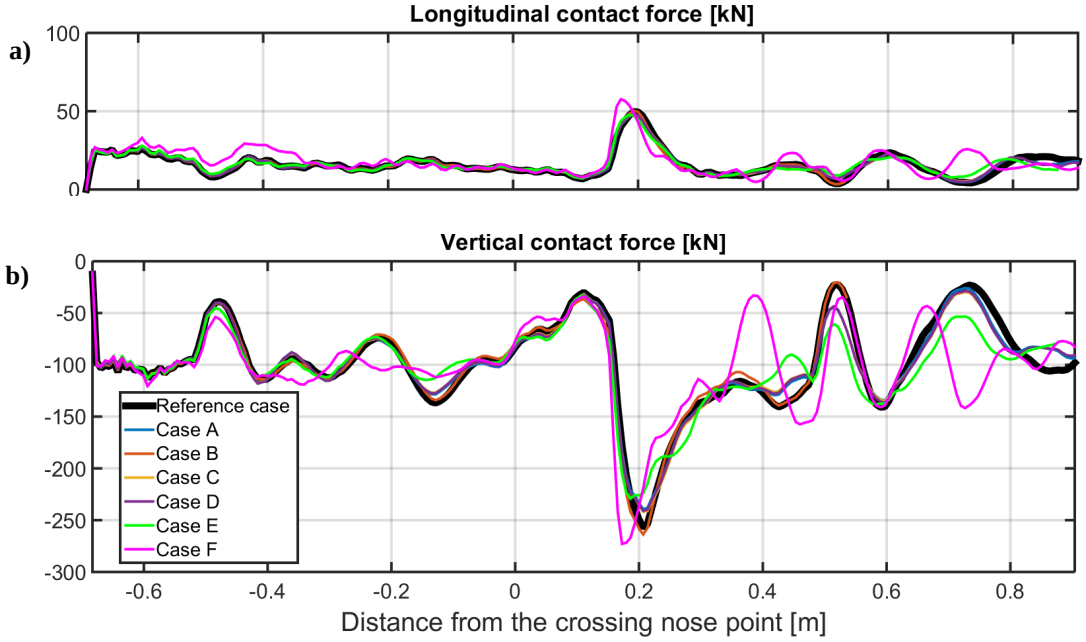

Figure 44. Contact force comparison for the investigated case studies. a) Longitudinal contact force; b) vertical contact force

5.3. Geometric design improvement

As presented in Section 3.4.5, the impact event is mainly induced by the abrupt change in the vertical movement of the wheel. This could be because of bad vertical track stiffness, as discussed in the previous subsection, but also because of poor interaction of the wheel-crossing bodies. The latter case is investigated here, in which the standard crossing profiles are modified in order to achieve a better wheel-crossing interaction which enables a smooth passage of the wheel in the transition zone. This problem has been addressed in the literature by many researchers using different optimization methods integrated with MBS simulations [30-32]. However, in this case the coupling strategy is utilized which enables modifications to be done to the initial models and updating them to assess the design modifications based on FE dynamic simulations.

5.3.1. Design criteria and computational strategy

The design criterion followed here to judge the acceptability of a design modification is mainly based on smoothening of the vertical wheel trajectory because this provides a good and quick reflection of the impact behaviour.
In order to make the computation fast and efficient, first, the parameterised cross sectional drawings are modified in AutoCAD and exported into the 2D geometric model for contact simulation. The wheelset is placed on a cross section of the crossing panel to calculate the contact conditions. After doing this process for multiple cross sections along the crossing panel, the vertical wheel trajectory can be extracted to see whether the geometric modification agrees with the mentioned design criterion. If not additional modification is performed in AutoCAD and the vertical wheel trajectory is calculated again. If the design criteria are meet than, the 3D-FE model is updated according to the selected design modification and finally, dynamic simulation is performed to assess the dynamic behaviour of the design.

5.3.2. Basic case studies

Optimizing the crossing geometry includes many design variables which should be taken in to account. A balanced approach for crossing geometry improvement requires considering both the wheel and crossing profiles because in reality the wheel shape profiles have different wheel tread conicities varying from 1/20 up to even negative conicity (hollow wheel tread). The vertical wheel trajectory is a function of lateral displacement of the wheel, which in turn is again a function of the wheel and the crossing profiles. Although the 2D geometric model is flexible enough to include modification of both wheel and crossing profiles, such an extensive research does not fit within the time frame of this MSc thesis. Therefore, in this work only standard wheel profile S1002 is considered and zero lateral shift of the wheel. As for the crossing profiles, since the focus of this study is primarily on

reducing the impact forces in the transition zone, only the transition profiles of the crossing panel are modified.
In the literature it has been reported [33-35] that the so called MaKüDe design, in which the wing rail head is profiled with contra wheel shape, results in better wheel-rail performance. In order to investigate this claim, two basic design modifications are studied namely;

- Design A_0**:** 1/20 inclined wing rail head.
- Design B_0**:** 1/40 inclined wing rail head.

5.3.3. 2D-geometric contact simulation results

For these two design modifications, the 2D-geometric contact simulation has been performed. Figure 45a-b shows the geometric adjustments made with respect to the standard drawing and their corresponding vertical wheel trajectory. It can be observed that due to the inclined wing rail head, the vertical wheel drop has been increased significantly. Moreover, the lowest point of the wheel drop occurs closer to the front of the crossing nose compared with the reference case.

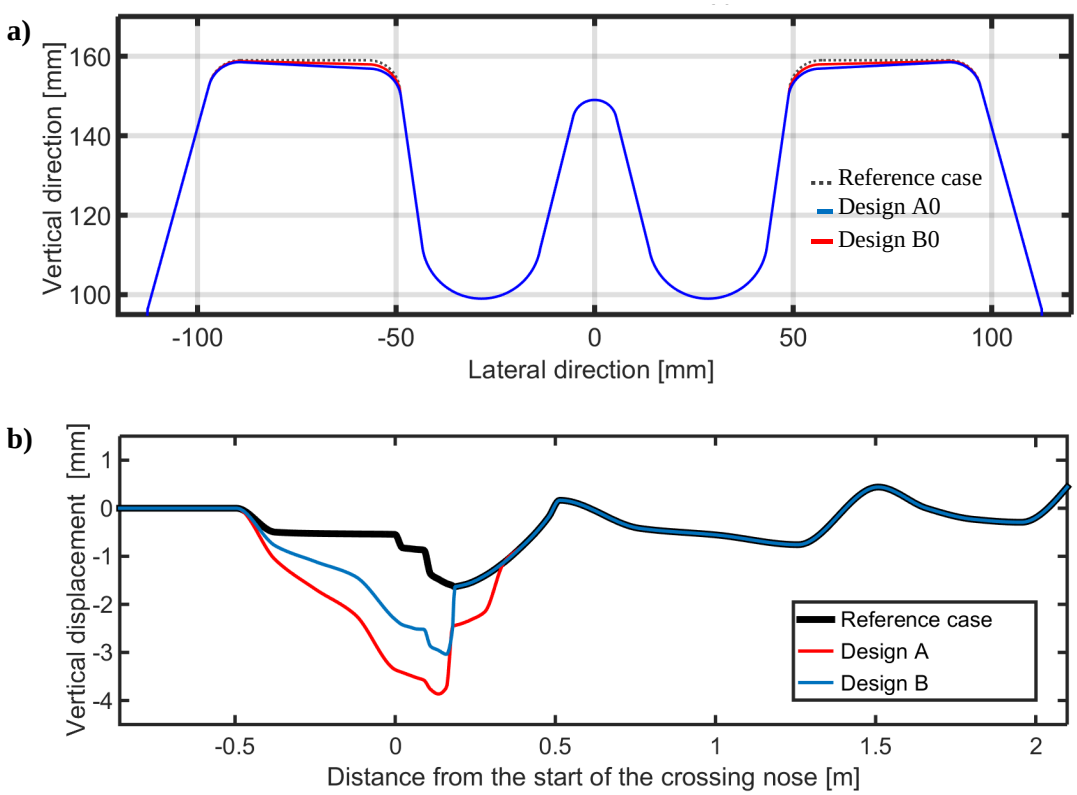

Figure 45. a) Geometric design modification Design A_0 & B_0; b) Vertical movement of the wheel axle for zero lateral displacement.

From Figure 45b it was observed that even small adjustment of the contacting geometries can lead to significant change in the vertical movement of the wheel. In order to improve the vertical trajectory of the wheel, the designs A_0 & B_0 are taking as starting point for further modification. Table 7-8 shows four additional case studies (A_1 to A_2 & B_1 to B_2) which are further improvements made to the basic Design A_0 & B_0. The values within the brackets indicate the changes made relative to the reference case, see Figure 46a-b (next page) for the graphical representation of some cross sections.

Table 7. Design A. Modification of cross sectional data w.r.t the reference case

Cross section	**Slope wing rail**	**Wing rail height [mm]**			**Height crossing nose [mm]**		
		[A_0]	[A_1]	[A_2]	[A_0]	[A_1]	[A_2]
DD_0	1/20	[-]	[+4]	[+4]	[-]	[-]	[-]
DD_90	1/20	[-]	[+4]	[+4]	[-]	[-]	[-]
DD_180	1/20	[-]	[+4]	[+4]	[-]	[-]	+2.5
EE	1/20	[-]	[+4]	[+4]	[-]	[-]	[-]

Table 8. Design B. Modification of cross sectional data w.r.t the reference case

Cross section	**Slope wing rail**	**Wing rail height [mm]**			**Height crossing nose [mm]**		
		[B_0]	[B_1]	[B_2]	[B_0]	[B_1]	[B_2]
DD_0	1/40	[-]	[+4]	[+4]	[-]	[-]	[-]
DD_90	1/40	[-]	[+4]	[+4]	[-]	[-]	[-]
DD_180	1/40	[-]	[+4]	[+4]	[-]	[-]	+2.5
EE	1/40	[-]	[+4]	[+4]	[-]	[-]	[-]

In the Design A_1 & B_1, the wing rail head has been increased by 4 mm. From the vertical wheel movement shown in Figure 46c, it can be seen that the wheel drop has been changed into a vertical hill. This situation is more favourable than the reference case because the slope of the wheel trajectory is less steep which means that accelerations are lower. However, at ***I*** and ***II*** locations the vertical wheel trajectory have still some steep gradients especially for design B_1.

In order to counteract this effect, height of the nose for the cross section DD_180 has been increased by 2.5 mm in the Design A_2 & B_2. Through this modification it can be seen that indeed the wheel trajectory has been smoothen effectively.

In short it can be concludes that the Design A_2 & B_2 both results in a smooth vertical movement of the wheel for the given S1002 wheel profile. However Design A_2 is preferable in this case because the vertical displacement is much smaller. This design agrees well with the design criteria mentioned earlier and as such, it is selected for further investigation based on the 3D finite element analysis.

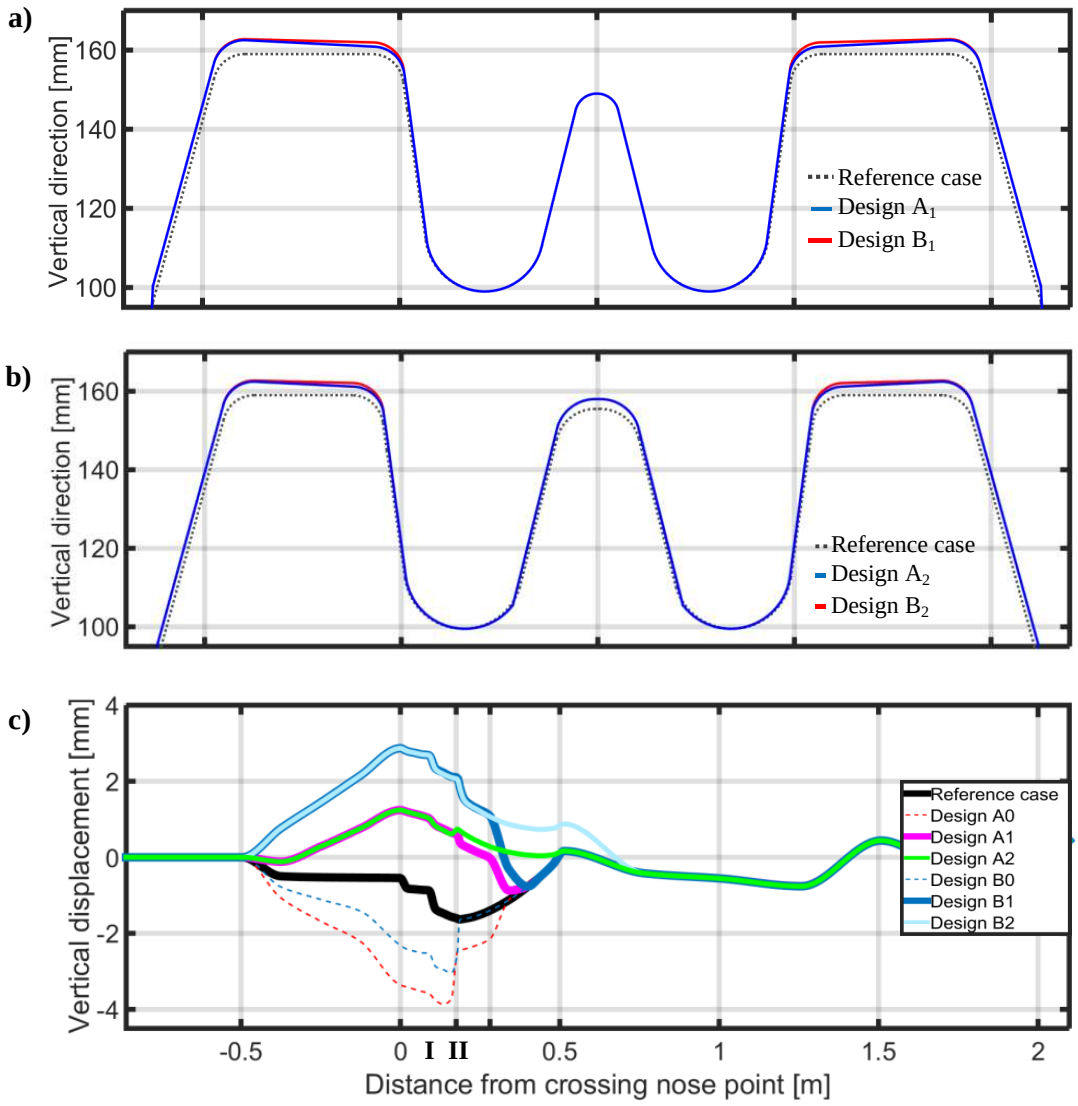

Figure 46. a) Design A_1 & B_1. Shown for the cross section at 90 mm after crossing nose front; b) Design A_2 & B_2. Shown for the cross section at 180 mm after crossing nose front; c) Vertical wheel trajectory for all the design

5.3.4. 3D Finite element simulation result

It was concluded in the previous section that from the investigated cases the Design A_2, causes the wheel to make the smoothest transition. However, the calculation of the vertical wheel trajectory was based on static contact simulation. In this section, dynamic finite element simulation is performed to examine the whether the predicted wheel trajectory is true and whether the contact forces are influenced. In order to verify this, the FE model is updated according to the Design A_2. Figure 47b-c shows the wing rail head for the original model as well as the updated FE model. See Appendix B for a complete overview of the modified transition cross sections.

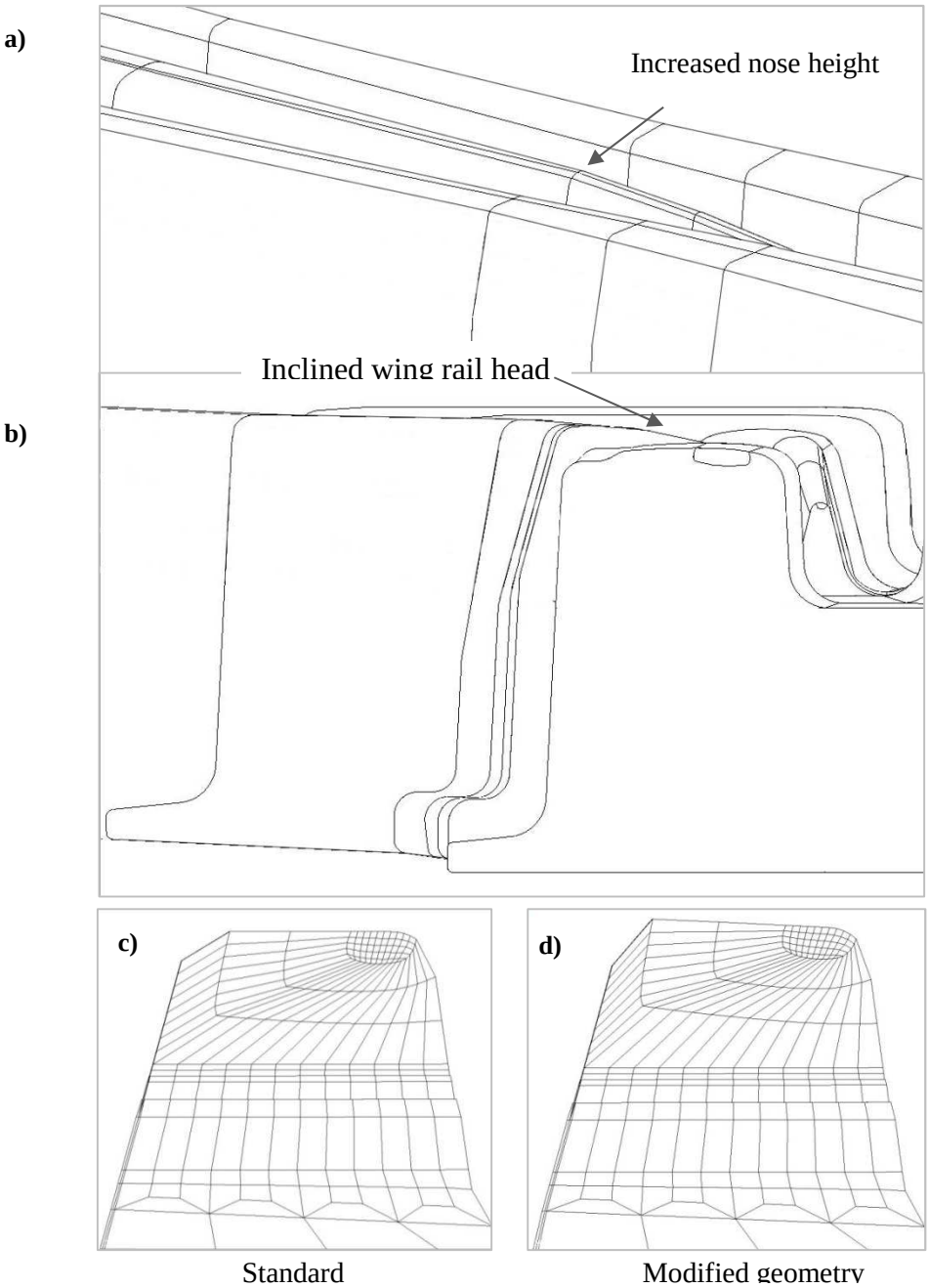

Figure 47: The FE model has been updated according to Design A_2; a-b) Updated solid model; c) Meshed model. Standard wing rail head; d) Meshed model. Modified wing rail head

Utilizing the modified geometry, dynamic simulation is carried out according to the procedure described in Section 3.4. The calculated contact forces and vertical wheel trajectory are shown in Figure 48. It can be seen from Figure 48a that indeed, as it was predicted by the 2D geometric model, the wheel makes now a upwards movement instead of a downward movement. Besides, compared with the reference case the irregularities in the vertical wheel movement has been effectively mitigated. Due to this, it can be observed from Figure 48b-c that contact forces oscillation is now more stable and, at the moment of impact the vertical contact force has been lowered almost two times. However, due to the increased nose height, the wheel is still striking against the crossing nose, the result of which is that the magnitude of the shear force has not been influenced too much.

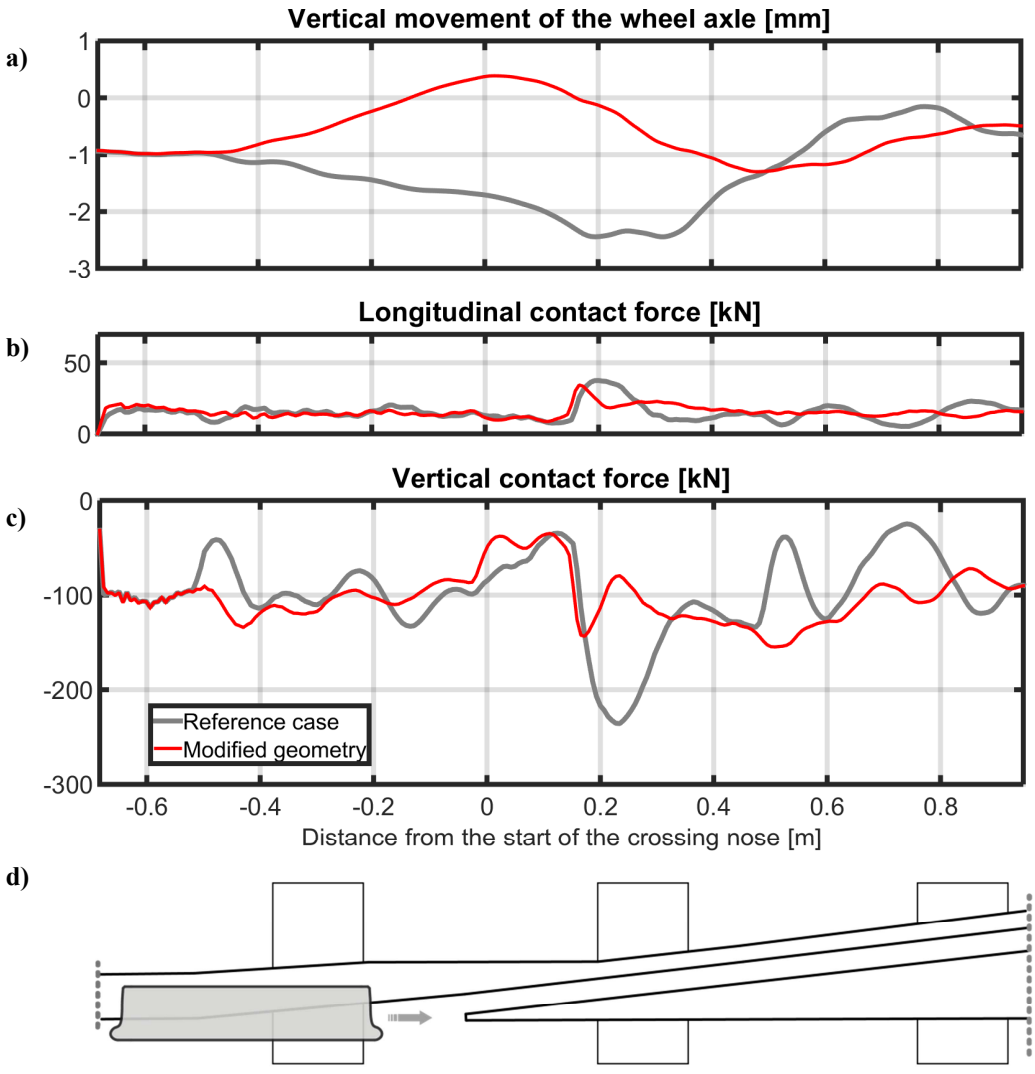

Figure 48: a) Longitudinal contact force w.r.t rolling distance; b) Vertical contact force w.r.t rolling distance; c) Vertical wheel trajectory; d) top view of the wheel and the crossing panel

A comparison of the Von Mises stress distribution for standard and modified geometry at the moment of impact is presented in Figure 49. It can be noticed that the maximum Von Mises stress is higher for modified geometry. This is because the impact occurs closer to the crossing nose front where the curvature of the nose is still small, resulting in relatively smaller contact patch. Looking at the subsurface stress distribution it can be noted that maximum stress state is located more at the top surface of material compared with the standard case.

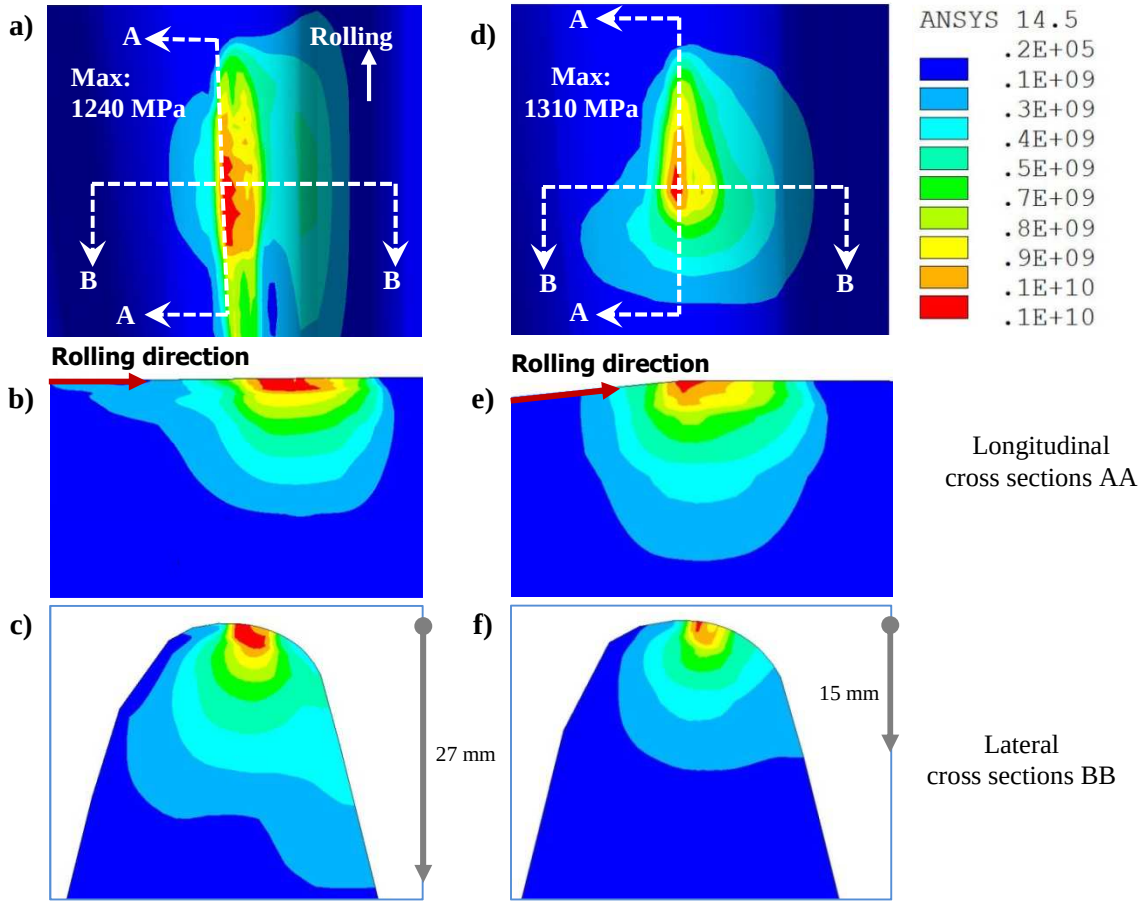

Figure 49. a) Standard geometry. VM surface stress at 223mm from the crossing nose front; b) Cutting plane AA; c) Cutting plane BB; d) Modified geometry. VM surface stress at 180mm from the crossing nose front; e) Cutting plane AA; f) Cutting plane BB;

In short, it can be concluded that the investigated Design A_2 results in a smoother vertical wheel movement compared with the standard case for the standard S1002 wheel profile and zero lateral wheel shift. Dynamic finite element simulation revealed that the contact forces has been reduced effectively while the local stresses at the impact moment has been slightly increased. The presented stress state is only for one wheel passage however, multiple wheel passage will cause plastification at the contact area which will result in more conformal contact and stress reduction. Therefore, the modified geometry provide good opportunity for a better wheel-rail performance but additional investigation is needed to confirm this.

5.4. Facing vs trailing direction

Until now, all the simulations were performed for the facing direction. However, in reality the trains can approach the crossing from different directions. When an approaching train passes first on the wing rail before it makes the transition to the crossing nose, this called facing direction. When a train passes first on the crossing nose before it arrives at the wing rail then that is considered the trailing direction, see Figure 50c. In order to investigate the contact force distribution for these two operational conditions, additional simulation in the trailing direction is performed with the same FE model. The comparison is done for trailing and facing direction is done for standard crossing profiles as well as for the modified profiles.

5.4.1. Comparison for standard profiles

The simulation results for the facing direction has already proceeded in Section 3.4. As for the trailing direction, the wheel is initially placed at cross-section EE which is 0.513m away from the front of the crossing nose. Figure 50 shows the results from explicit simulation for standard crossing profiles. From the results it can be seen that the impact occurs at different longitudinal location, but the magnitude of this contact force is the same order. However from the vertical wheel trajectory it is apparent that in the trailing direction more vertical movement of the wheel axle takes place. Besides, it can be observed that the contact force oscillation for both case are in the same frequency range.

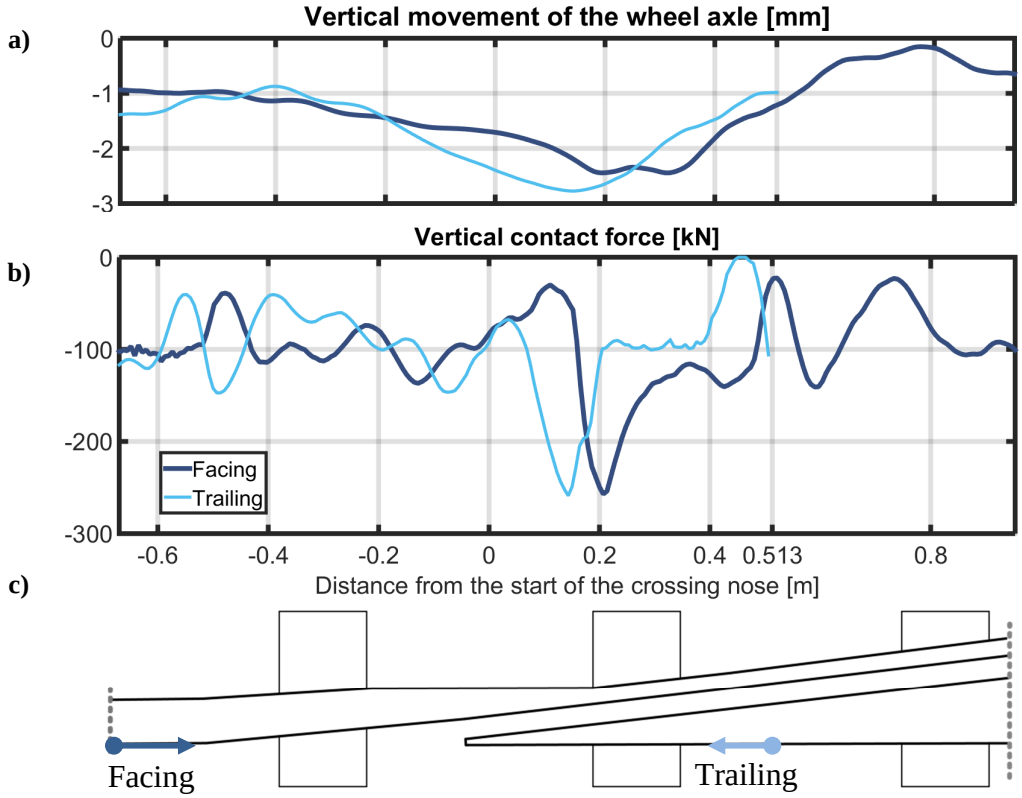

Figure 50. Comparison between facing and trailing direction. a) Vertical contact force. b) Vertical displacement of the wheel axle. c) top view crossing panel

5.4.2. Comparison for modified geometry

In this section, a comparison for the facing and the trailing direction is made utilizing modified crossing geometry as introduced in Section 5.3.3. The results presented in Figure 51 are of similar trend to the standard geometry. However, some specific interesting notes can be made, from them, the impact location for facing and trailing direction has been shifted more towards the front of the crossing nose whilst the impact force has been slightly larger for the trailing direction. Moreover, a large contact force oscillation has been introduced at the wing rail at -0.5m for the trailing direction. It should be underlined from this that during the design process both directions should be verified to make sure that railway operation is possible for both directions and undesirable effect, if any are known.

Based on this, it can be concluded that the geometric design modification has introduced a small impact force but the magnitude of the impact forces in general has been reduced significantly compared with the standard geometry, see Figures 50a-b.

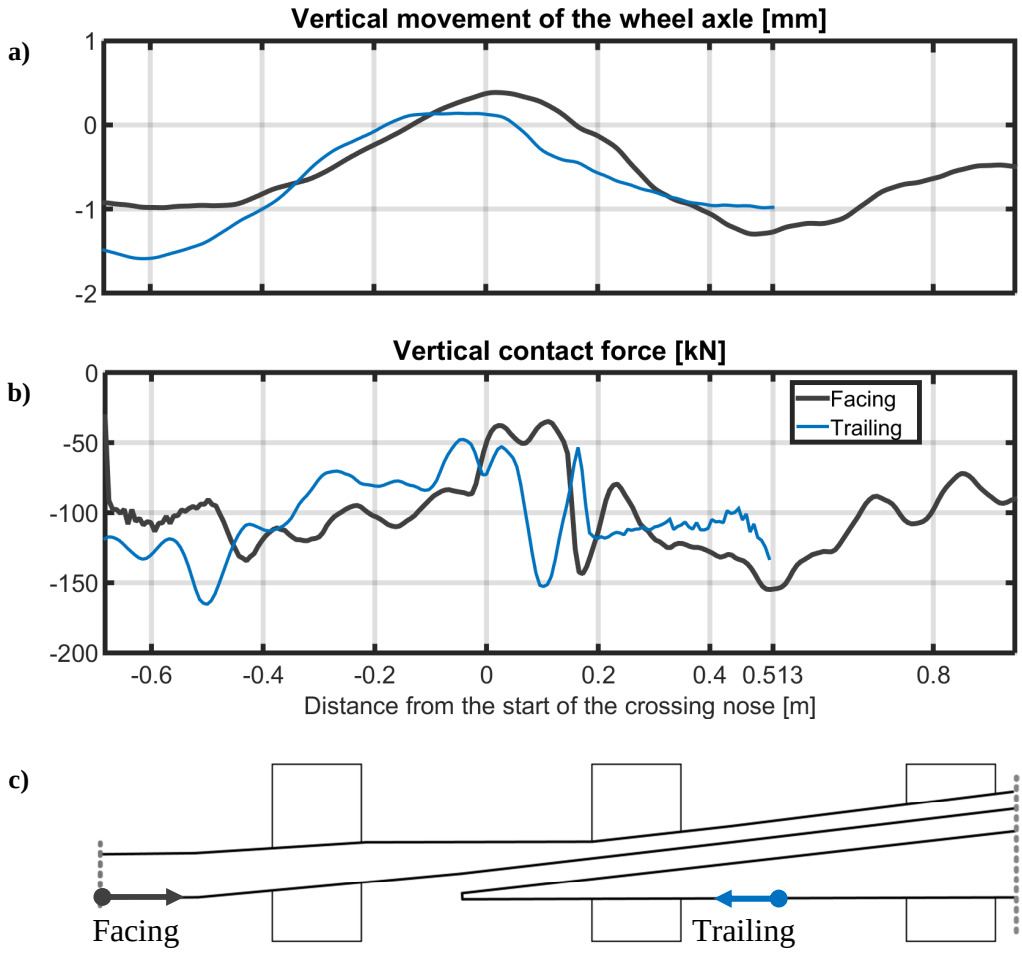

Figure 51. Comparison between facing and trailing direction for Design A_2 . a) Vertical contact force. b) Vertical displacement of the wheel axle. c) top view crossing panel

6.

Conclusions

In this MSc thesis, a 3D finite element (FE) model for analysing and improving the wheel-crossing contact interaction was developed. To increase the efficiency of the FE model, a coupling strategy with the 2D geometric model is proposed. Based on the presented results and discussions, the following conclusions can be made:

1). Successful modelling and simulating wheel-crossing interaction requires information about the wheel-rail contact conditions and the relative positioning between wheel and crossing. The presented 2D geometric model, is able to calculate and prepare all the required data to build a detailed and realistic finite element model of the crossing panel.

2). The developed FE model is capable to capture high rolling contact stresses resulting from dynamic impact in the transition zone. At the moment of impact, contact stresses exceed 2.5 times the yield stress leading to work hardening. Subsurface stress analysis revealed that the high stress state is concentrated in rather a small volume of material producing intense plastic strain increase the likelihood of crack initiation which correlates quite well with field observations.

3). A comparison of the accelerations of the wheel and the crossing showed that the FE model and the field measurement have some conformities as well as discrepancies. The magnitude of the impact accelerations from the FE model and the field experiment are comparable while there is some mismatch in the frequency range of the two signals which could be because of unknown parameters and simplifications of the FE model.

4). By conducting the parametric study it was shown that contact stresses resulting from an impact event can be captured more adequately using plastic material model. However, there is a relatively minor difference in contact force distribution between elastic and plastic calculations, which provides the opportunity to assess contact forces using simple linear elastic calculations.

5). Moreover, in the parametric study it was highlighted that the vertical track stiffness provides potentials for reducing the high contact forces. In this regards, the

most effective measure to do so is selecting relatively softer rail pads and lighter sleepers for three supports in the vicinity of the transition zone.

6). A more effective and more challenging potential to reduce impact loads and ensure a smooth transition is through crossing geometric design improvement. As it was shown, providing that the lateral displacement of the wheelset is limited as well as the spreading between the different wheel profiles, impact loads can be mitigated effectively by elevating the wing rail and profiling it with inclined railhead of 1/20.

7). A comparison between facing and trailing simulation showed that impact event occurs at different location of the crossing panel, but the magnitude of this impact force is more or less the same. Moreover, it was shown that the geometric design modification as explained above also mitigates the impact force for the trailing direction.

Finally, the FE model can be further improved to simulate more accurately the physical reality, after which it can contributes to a better design of the crossing panel and relative assessment of the contact forces and its resulting stress/strain response.

Reference

[1] H. Sugiyama, Y. Tanii, and R. Matsumura, "Analysis of Wheel/Rail Contact Geometry on Railroad Turnout Using Longitudinal Interpolation of Rail Profiles," *Journal of Computational and Nonlinear Dynamics,* vol. 6, p. 024501, 2011.

[2] M. Wiest, E. Kassa, W. Daves, J. C. O. Nielsen, and H. Ossberger, "Assessment of methods for calculating contact pressure in wheel-rail/switch contact," *Wear,* vol. 265, pp. 1439-1445, 10/30/ 2008.

[3] A. Johansson, B. Pålsson, M. Ekh, J. C. O. Nielsen, M. K. A. Ander, J. Brouzoulis, *et al.*, "Simulation of wheel–rail contact and damage in switches & crossings," *Wear,* vol. 271, pp. 472-481, 2011.

[4] M. Pletz, W. Daves, and H. Ossberger, "A wheel passing a crossing nose: Dynamic analysis under high axle loads using finite element modelling," *Proceedings of the Institution of Mechanical Engineers Part F-Journal of Rail and Rapid Transit,* vol. 226, pp. 603-611, Nov 2012.

[5] L. Xin, V. Markine, and I. Shevtsov, "Dynamic Interaction Between the Wheel and Crossing Nose," 2013.

[6] F. W. Carter, "On the action of a locomotive driving wheel.," *Proceedings of the Royal Society of London Series a-Containing Papers of a Mathematical and Physical Character,* vol. 112, pp. 151-157, Aug 1926.

[7] J. J. Kalker, "Three-dimensional elastic bodies in rolling contact Kluwer Academic Publishers," *Dordrecht,* 1990.

[8] K. Johnson, "Contact Mechanics Cambridge University Press London," ed: UK, 1985.

[9] O. Polach, "A fast wheel-rail forces calculation computer code," *Vehicle System Dynamics,* vol. 33, pp. 728-739, 2000.

[10] INNOTRACK, "The state of the art of the simulation of vehicle track interaction as a method for determining track degradation rates. Part 2 – High Resolution models and the level of validation generally," *Deliverable report D1.3.6,* pp. 1-33, 2009.

[11] H. Hertz, "Über die Berührung fester elastischer Körper," *Journal für die reine und angewandte Mathematik,* vol. 92, pp. 156-171, 1882.

[12] S. Z. Meymand, A. Keylin, and M. Ahmadian, "A survey of wheel–rail contact models for rail vehicles," *Vehicle System Dynamics,* vol. 54, pp. 386-428, 2016.

[13] J. J. Kalker, "A fast algorithm for the simplified theory of rolling contact," *Vehicle system dynamics,* vol. 11, pp. 1-13, 1982.

[14] E. Vollebregt, C. Weidemann, and A. Kienberger, "Use of “CONTACT” in multi-body vehicle dynamics and profile wear simulation: Initial results," in *Proceedings of the 22nd International Symposium on Dynamics of Vehicles on Roads and Tracks*, 2011.

[15] Y. Ma and V. L. Markine, "A Numerical Procedure for Analysis of W/R Contact Using Explicit Finite Element Methods," presented at the 10th International Conference on Contact Mechanics, Colorado, 2015.
[16] E. Kassa, C. Andersson, and J. C. Nielsen, "Simulation of dynamic interaction between train and railway turnout," *Vehicle System Dynamics,* vol. 44, pp. 247-258, 2006.
[17] M. Pletz, W. Daves, and H. Ossberger, "A wheel passing a crossing nose: Dynamic analysis under high axle loads using finite element modelling," *Proceedings of the Institution of Mechanical Engineers, Part F: Journal of rail and rapid transit,* p. 0954409712448038, 2012.
[18] J. Xu, P. Wang, L. Wang, and R. Chen, "Effects of profile wear on wheel–rail contact conditions and dynamic interaction of vehicle and turnout," *Advances in Mechanical Engineering,* vol. 8, p. 1687814015623696, 2016.
[19] A. Johansson, B. Pålsson, M. Ekh, J. C. Nielsen, M. K. Ander, J. Brouzoulis, *et al.*, "Simulation of wheel–rail contact and damage in switches & crossings," *Wear,* vol. 271, pp. 472-481, 2011.
[20] CEN, "Railway applications-Wheelsets and bogies- Wheels-Tread profile, European Standard," ed, 2006.
[21] U. CODE, "515-1 OR," in *Passenger rolling stock - trailer bogies - running gear - General provisions applicable to the components of trailers bogies,* ed, 2003.
[22] Y. Ma, M. Ren, G. Hu, and C. Tian, "Optimal analysis on rail pre-grinding profile in high-speed railway," *Jixie Gongcheng Xuebao(Chinese Journal of Mechanical Engineering),* vol. 48, pp. 90-97, 2012.
[23] M. Hiensch, J. C. Nielsen, and E. Verheijen, "Rail corrugation in the Netherlands—measurements and simulations," *Wear,* vol. 253, pp. 140-149, 2002.
[24] T. Telliskivi and U. Olofsson, "Contact mechanics analysis of measured wheel-rail profiles using the finite element method," *Proceedings of the Institution of Mechanical Engineers, Part F: Journal of Rail and Rapid Transit,* vol. 215, pp. 65-72, 2001.
[25] V. Markine, M. Steenbergen, and I. Shevtsov, "Combatting RCF on switch points by tuning elastic track properties," *Wear,* vol. 271, pp. 158-167, 2011.
[26] X. Zhao and Z. Li, "The solution of frictional wheel–rail rolling contact with a 3D transient finite element model: Validation and error analysis," *Wear,* vol. 271, pp. 444-452, 5/18/ 2011.
[27] E. T. Selig and D. Li, "Track modulus: Its meaning and factors influencing it," *Transportation Research Record,* 1994.
[28] A. Lundqvist and T. Dahlberg, "Railway track stiffness variation-consequences and countermeasures," in *19th IAVSD Symposium of Dynamics of Vehicles on Roads and Tracks, Milano, August 29-Seprember 2, 2005,* 2005.
[29] I. Grossoni, Y. Bezin, and S. Neves, "Optimization of support stiffness at a railway crossing panel," 2016.
[30] B. A. Pålsson, "Optimisation of railway crossing geometry considering a representative set of wheel profiles," *Vehicle System Dynamics,* vol. 53, pp. 274-301, 2015.

[31] C. Wan, V. Markine, I. Shevtsov, and R. Dollevoet, "Improvement of train-track interaction in turnouts by optimising the shape of crossing nose," in *IAVSD 2013: 23rd International Symposium on Dynamics of Vehicles on Roads and Tracks, Qingdao, China, 19-23 August 2013*, 2013.

[32] V. Markine and I. Shevtsov, "An Experimental Study on Crossing Nose Damage of Railway Turnouts in The Netherlands," in *Civil-Comp Proceedings: Proceedings of the 14th International Conference on Civil, Structural and Environmental Engineering Computing, Cagliari, Sardinia, Italy, 3-6 September 2013; paper 37*, 2013.

[33] U. BjörnPaulsson, J. Jaiswal, and A. Ekberg, "The EU-project INNOTRACK–a description of highlights and how they have been implemented."

[34] D. Nicklisch, E. Kassa, J. Nielsen, M. Ekh, and S. Iwnicki, "Geometry and stiffness optimization for switches and crossings, and simulation of material degradation," *Proceedings of the Institution of Mechanical Engineers, Part F: Journal of Rail and Rapid Transit*, vol. 224, pp. 279-292, 2010.

[35] B. Asmussen, "Description of the vibration generation mechanism of turnouts and the development of cost effective mitigation measures," *Railway Induced Vibration Abatement Solutions Collaborative Project (RIVAS)*, 2013.

Appendix

Appendix A – Standard crossing panel cross sections
1/9 Cast Manganese crossing.

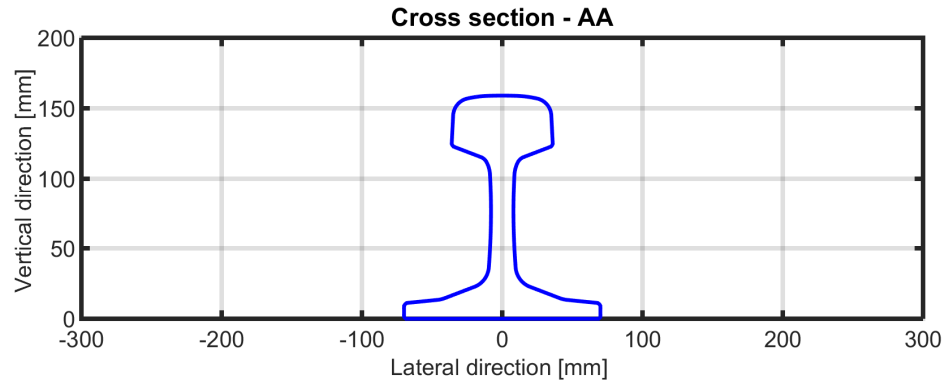

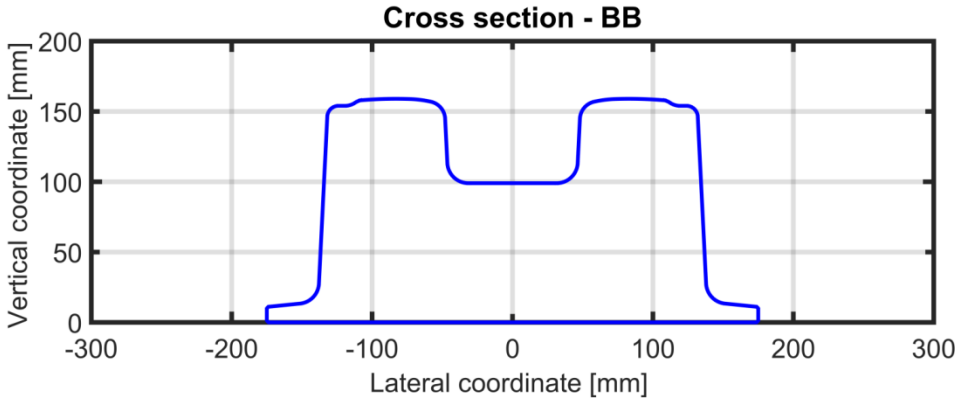

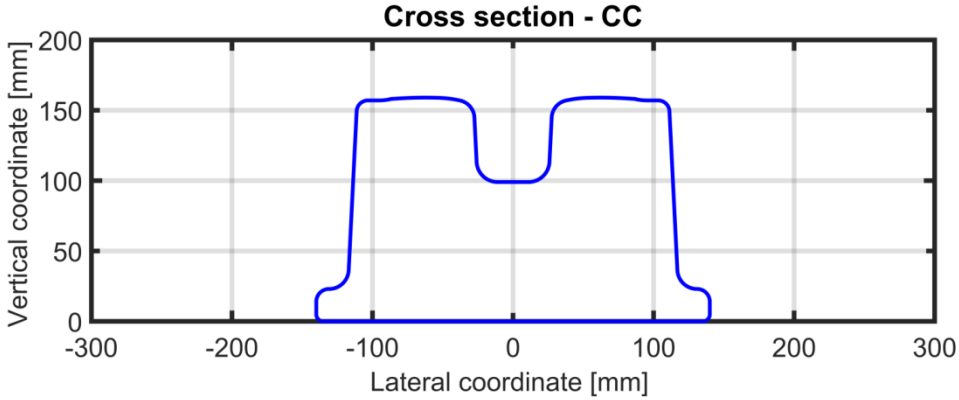

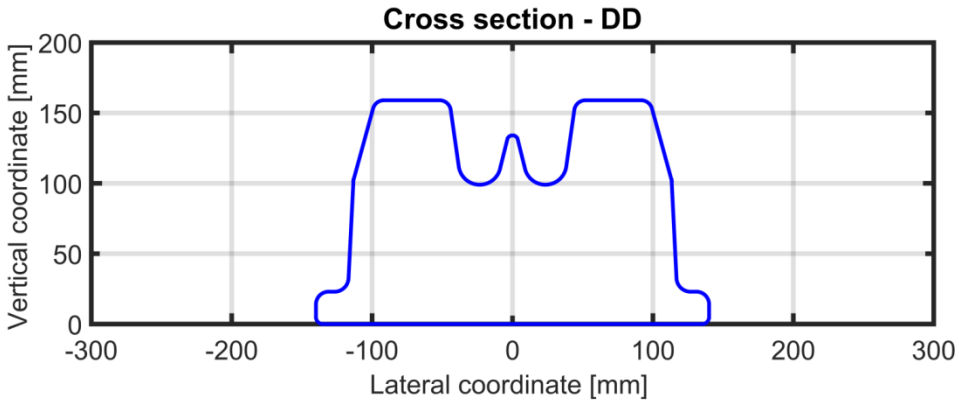
Cross section - DD
Vertical coordinate [mm]
200
150
100
50
0
-300
-200
-100
0
100
200
300
Lateral coordinate [mm]

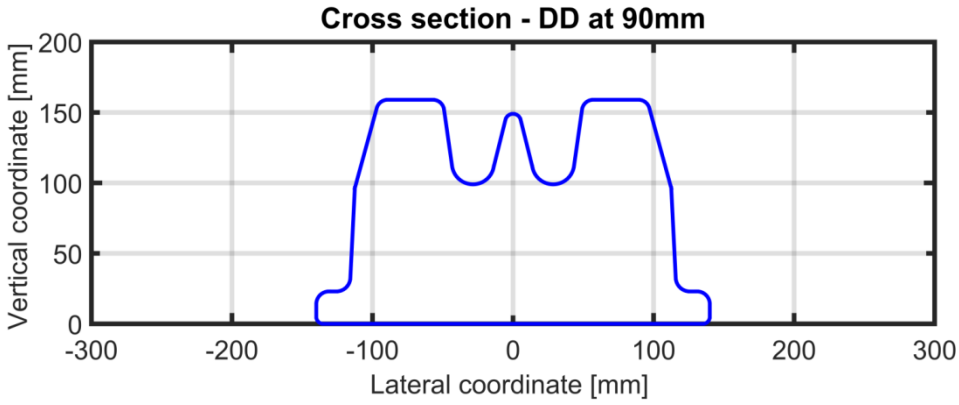
Cross section - DD at 90mm
Vertical coordinate [mm]
200
150
100
50
0
-300
-200
-100
0
100
200
300
Lateral coordinate [mm]

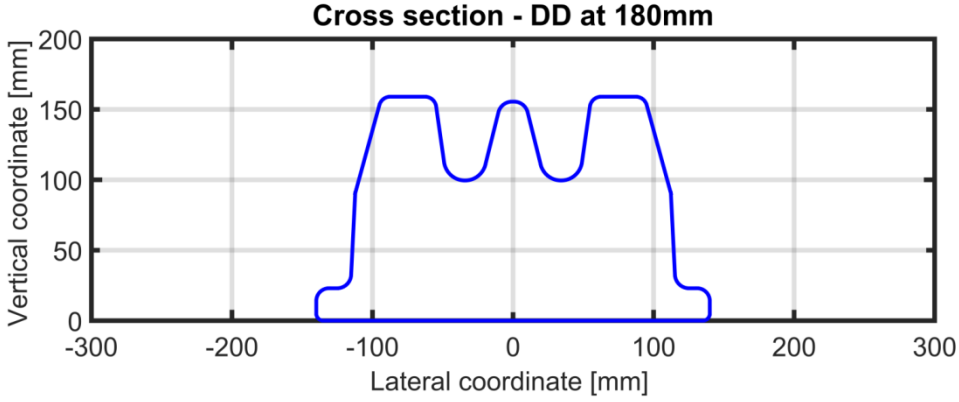
Cross section - DD at 180mm
Vertical coordinate [mm]
200
150
100
50
0
-300
-200
-100
0
100
200
300
Lateral coordinate [mm]

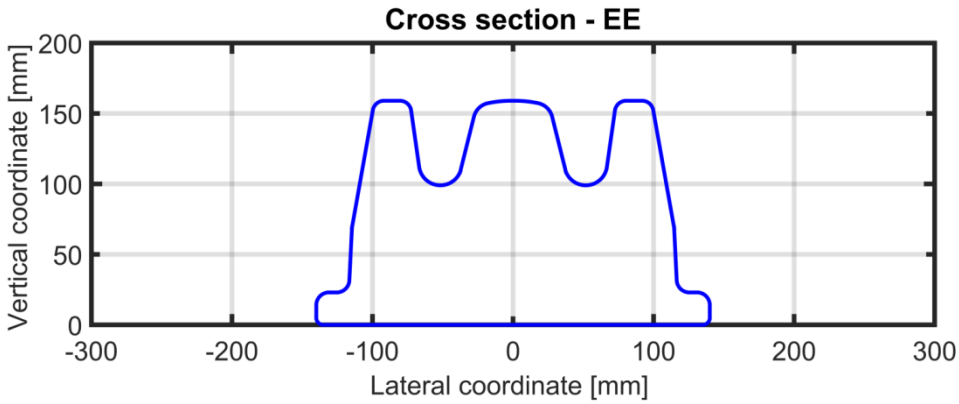
Cross section - EE
Vertical coordinate [mm]
200
150
100
50
0
-300
-200
-100
0
100
200
300
Lateral coordinate [mm]

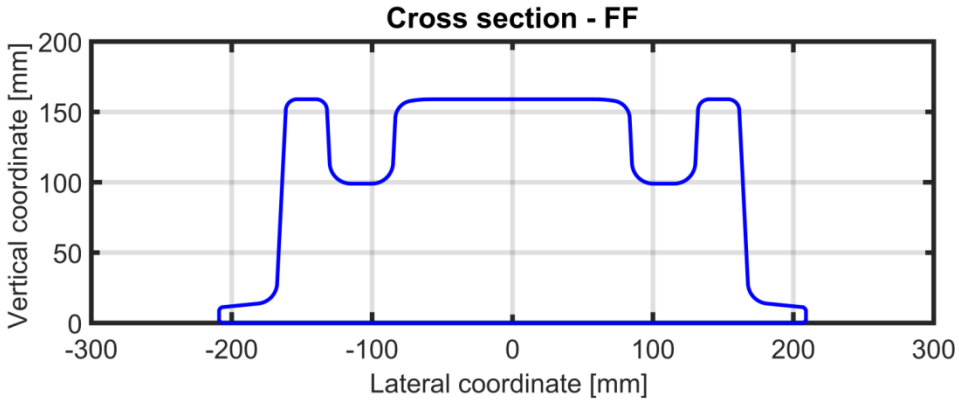
Cross section - FF
Vertical coordinate [mm]
200
150
100
50
0
-300
-200
-100
0
100
200
300
Lateral coordinate [mm]

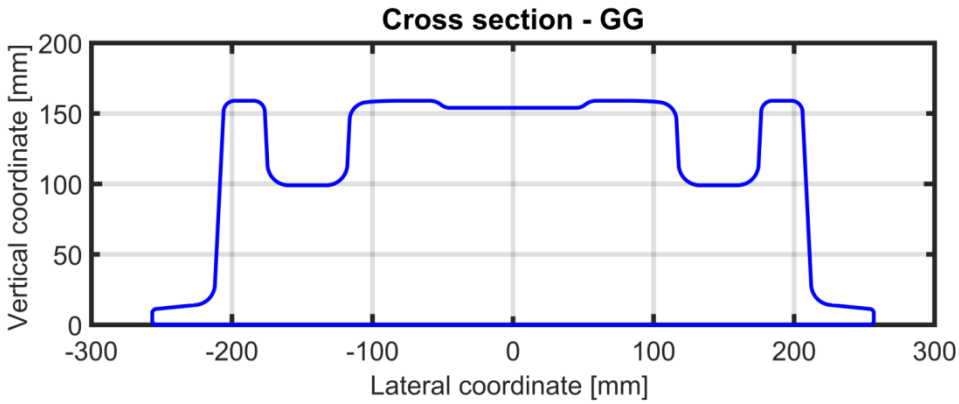
Cross section - GG
Vertical coordinate [mm]
200
150
100
50
0
-300
-200
-100
0
100
200
300
Lateral coordinate [mm]

Appendix B – Modified transition cross sections

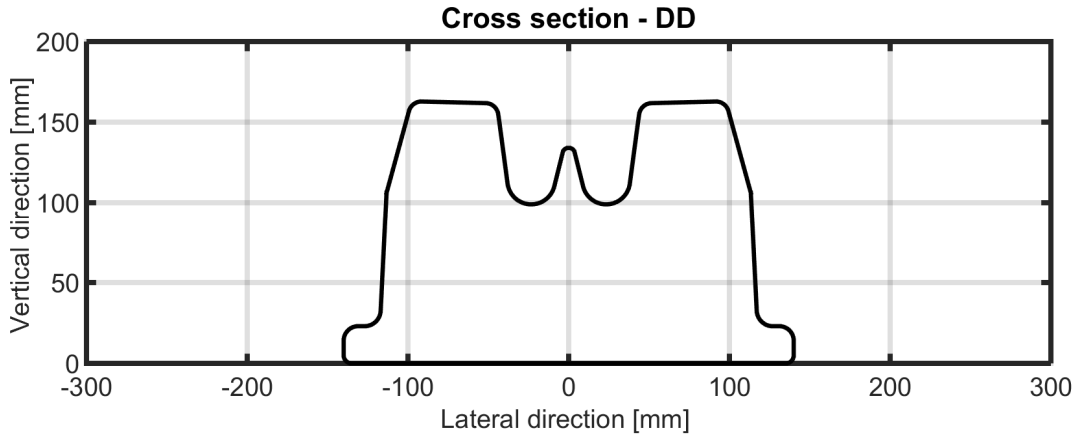

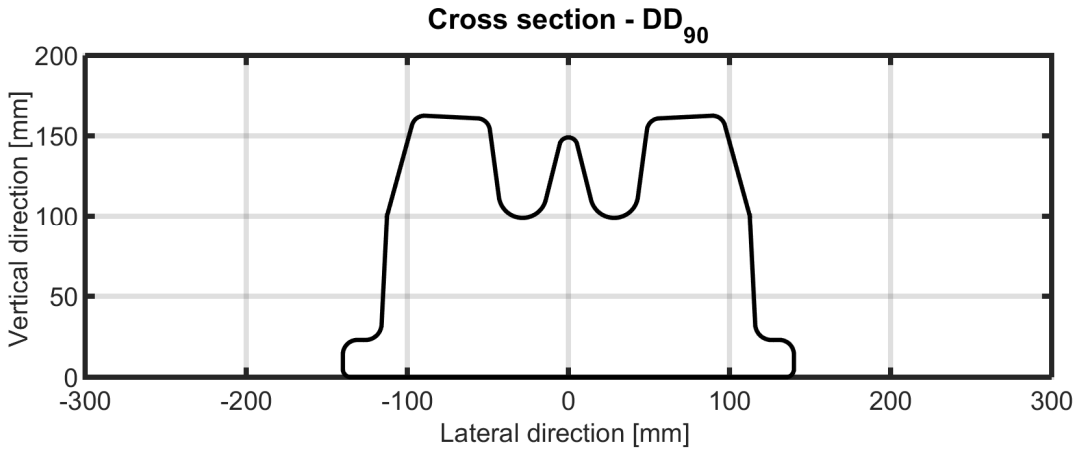

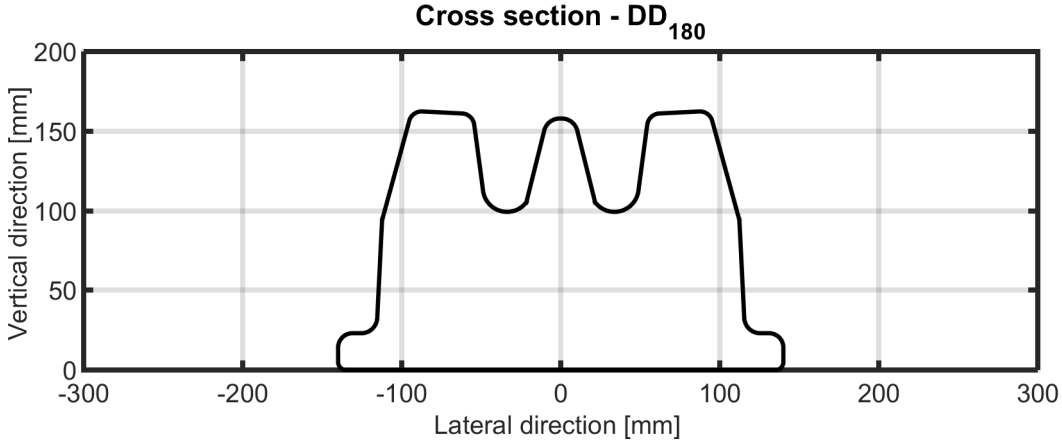

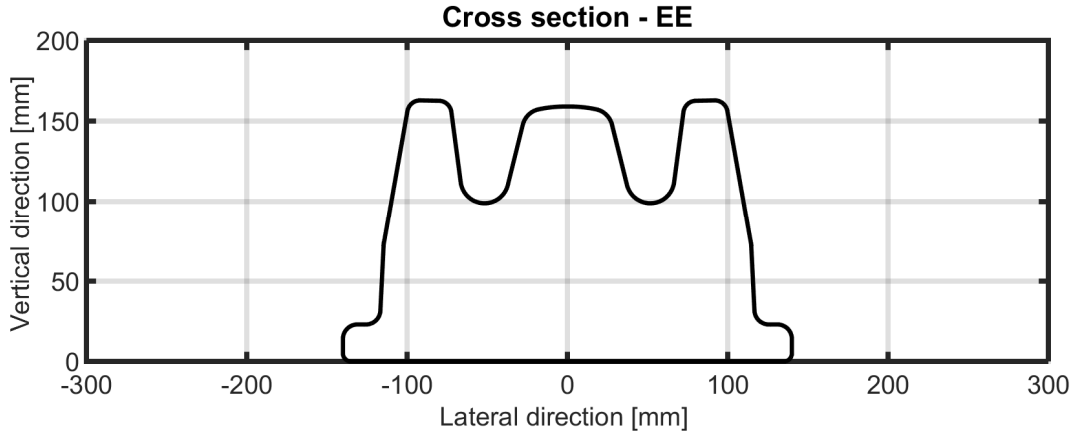

NOTE: Cross sections BB, CC, FF and GG are similar to the standard cross section, see Appendix A